NAVAL POSTGRADUATE SCHOOL

MONTEREY, CALIFORNIA

THESIS

MODEL DEVELOPMENT FOR WIRELESS PROPAGATION IN FORESTED ENVIRONMENTS

by

Jesus Zegarra

September 2015

Thesis Advisor:	David C. Jenn
Second Reader:	Phillip E. Pace

Approved for public release; distribution is unlimited

THIS PAGE INTENTIONALLY LEFT BLANK

REPORT DOCUMENTATION PAGE			*Form Approved OMB No. 0704–0188*
Public reporting burden for this collection of information is estimated to average 1 hour per response, including the time for reviewing instruction, searching existing data sources, gathering and maintaining the data needed, and completing and reviewing the collection of information. Send comments regarding this burden estimate or any other aspect of this collection of information, including suggestions for reducing this burden, to Washington headquarters Services, Directorate for Information Operations and Reports, 1215 Jefferson Davis Highway, Suite 1204, Arlington, VA 22202-4302, and to the Office of Management and Budget, Paperwork Reduction Project (0704-0188) Washington, DC 20503.			
1. AGENCY USE ONLY ***(Leave blank)***	**2. REPORT DATE** September 2015	**3. REPORT TYPE AND DATES COVERED** Master's thesis	
4. TITLE AND SUBTITLE MODEL DEVELOPMENT FOR WIRELESS PROPAGATION IN FORESTED ENVIRONMENTS			**5. FUNDING NUMBERS**
6. AUTHOR(S) Zegarra, Jesus			
7. PERFORMING ORGANIZATION NAME(S) AND ADDRESS(ES) Naval Postgraduate School Monterey, CA 93943-5000			**8. PERFORMING ORGANIZATION REPORT NUMBER**
9. SPONSORING /MONITORING AGENCY NAME(S) AND ADDRESS(ES) N/A			**10. SPONSORING / MONITORING AGENCY REPORT NUMBER**
11. SUPPLEMENTARY NOTES The views expressed in this thesis are those of the author and do not reflect the official policy or position of the Department of Defense or the U.S. Government. IRB Protocol number ____N/A____.			
12a. DISTRIBUTION / AVAILABILITY STATEMENT Approved for public release; distribution is unlimited			**12b. DISTRIBUTION CODE**

13. ABSTRACT (maximum 200 words)

Wireless propagation modeling is a necessary task in the design of countless applications. Wireless signals attenuate at different rates according to the propagation environment. Given that vegetation is an unavoidable feature for most outdoor wireless channels, propagation models in forested environments are in high demand. The characterization of radio waves propagating through foliage is particularly complex due to the random characteristics of the channel.

This research is focused on the development of three radiowave propagation models in forested environments. Field tests were performed at 2.4 GHz for the case where both the transmitting and receiving antennas are immersed in foliage. The propagation loss added by the forest component was estimated from the sets of measurement data, and an empirical model was created to forecast it. Also, electromagnetic properties of the medium were estimated and used in the investigation of a two-layered homogeneous model (ground and foliage). A dielectric slab representing the forest was modeled using an electromagnetic field simulation application.

Results from the empirical and analytical model show good agreement with the measured data. These findings bear direct relevance on radiowave propagation through foliage and provide useful information for accurate design of the link budget for similar scenarios.

14. SUBJECT TERMS radiowave propagation, forested environment, empirical modeling, analytical modeling, parameter estimation, attenuation			**15. NUMBER OF PAGES** 105
			16. PRICE CODE
17. SECURITY CLASSIFICATION OF REPORT Unclassified	**18. SECURITY CLASSIFICATION OF THIS PAGE** Unclassified	**19. SECURITY CLASSIFICATION OF ABSTRACT** Unclassified	**20. LIMITATION OF ABSTRACT** UU

NSN 7540–01-280-5500 Standard Form 298 (Rev. 2–89)
Prescribed by ANSI Std. 239–18

THIS PAGE INTENTIONALLY LEFT BLANK

Approved for public release; distribution is unlimited

MODEL DEVELOPMENT FOR WIRELESS PROPAGATION IN FORESTED ENVIRONMENTS

Jesus Zegarra
Lieutenant Junior Grade, Peruvian Navy
B. S., Peruvian Naval Academy, 2010

Submitted in partial fulfillment of the
requirements for the degree of

MASTER OF SCIENCE IN ELECTRICAL ENGINEERING

from the

NAVAL POSTGRADUATE SCHOOL
September 2015

Approved by: David C. Jenn
Thesis Advisor

Phillip E. Pace
Second Reader

R. Clark Robertson
Chair, Department of Electrical and Computer Engineering

THIS PAGE INTENTIONALLY LEFT BLANK

ABSTRACT

Wireless propagation modeling is a necessary task in the design of countless applications. Wireless signals attenuate at different rates according to the propagation environment. Given that vegetation is an unavoidable feature for most outdoor wireless channels, propagation models in forested environments are in high demand. The characterization of radio waves propagating through foliage is particularly complex due to the random characteristics of the channel.

This research is focused on the development of three radiowave propagation models in forested environments. Field tests were performed at 2.4 GHz for the case where both the transmitting and receiving antennas are immersed in foliage. The propagation loss added by the forest component was estimated from the sets of measurement data, and an empirical model was created to forecast it. Also, electromagnetic properties of the medium were estimated and used in the investigation of a two-layered homogeneous model (ground and foliage). A dielectric slab representing the forest was modeled using an electromagnetic field simulation application.

Results from the empirical and analytical model show good agreement with the measured data. These findings bear direct relevance on radiowave propagation through foliage and provide useful information for accurate design of the link budget for similar scenarios.

THIS PAGE INTENTIONALLY LEFT BLANK

TABLE OF CONTENTS

I. INTRODUCTION....1
A. COMPLEXITY OF A FORESTED ENVIRONMENT CHANNEL....1
B. EXISTING APPROACHES....3
C. THESIS OBJECTIVE....5
D. THESIS OUTLINE....5

II. MODELING PARAMETERS, TECHNIQUES AND METHODOLOGY....7
A. ELECTRICAL PROPERTIES OF THE MEDIA....7
B. ANALYTICAL METHODS FOR PATH MODELING AND LOSS PREDICTION....12
C. EMPIRICAL METHOD FOR PATH MODELING AND LOSS PREDICTION....19
1. Weissberger Model....20
2. International Telecommunication Union – Recommendation (ITU-R)....21
3. Fitted ITU-R (FITU-R) Model....21
4. Lateral ITU-R (LITU-R) Model....22
5. COST 235 Model....22
6. Seville Model....22
D. PLANE-EARTH MODEL....25
E. DEPOLARIZATION EFFECTS....26

III. EXPERIMENT DESIGN AND MEASUREMENT CAMPAIGN....27
A. EXPERIMENT SITE....27
B. EQUIPMENT AND MEASUREMENT SETUP....28
C. MEASUREMENT RESULTS....33

IV. PATH LOSS MODELING FROM EXPERIMENTAL DATA....37
A. MEASUREMENTS DISCUSSION....37
B. ATTENUATION CONSTANT ESTIMATION....39
C. EMPIRICAL PATH LOSS MODELING....43
D. LACK OF POLARIZATION DEPENDENCE....51

V. ANALYTICAL PATH LOSS MODELING OF PROPAGATION....53
A. PREVIOUS CONSIDERATIONS AND ASSUMPTIONS....53

B. MODEL FORMULATION....54
C. MODEL EVALUATION....58

VI. PATH LOSS MODELING WITH CEM SOFTWARE....61
A. GENERAL SETUP FOR SIMULATION OF RADIO WAVE PROPAGATION IN FOLIAGE....61
1. General Simulation Approach....61
2. Physical Construction....61
3. Solution settings....63
B. MODEL EVALUATION....64

VII. SUMMARY, CONCLUSIONS, AND RECOMMENDATIONS....69
A. SUMMARY....69
B. CONCLUSIONS....70
C. RECOMMENDATIONS....71

APPENDIX....73

LIST OF REFERENCES....81

INITIAL DISTRIBUTION LIST....85

LIST OF FIGURES

Figure 1. Different characteristics of forested environments (after [3]). 1

Figure 2. Simplified forest model and waves contributions (after [4]). 2

Figure 3. Stratified model of tropical rainforest (after [2]). 4

Figure 4. Attenuation of the magnitude of $E_x(z)$ as a function of distance z, (after [11]). 10

Figure 5. Propagation mechanisms in a three-layer model of the forest, (after [4]) 12

Figure 6. Propagation mechanisms for ground reflection problem (after [10]). 15

Figure 7. Excess loss versus distance at 2.4 GHz. 23

Figure 8. Excess loss versus frequency at 35.0 m foliage depth. 24

Figure 9. Experimental site satellite map. 27

Figure 10. Part of the measurement site at Fort Ord National Monument. 28

Figure 11. Transmitting and receiving antenna radiation patterns for vertical and horizontal polarizations (from [28]). 29

Figure 12. Schematic diagram of measurement setup (after [24]). 30

Figure 13. Measured power outside and inside the foliage block for vertically polarized antennas at 1.2 m. 33

Figure 14. Measured power outside and inside the foliage block for vertically polarized antennas at 2.0 m. 34

Figure 15. Measured power outside and inside the foliage block for horizontally polarized antennas at 1.2 m. 34

Figure 16. Measured power outside and inside the foliage block for horizontally polarized antennas at 2.0 m. 35

Figure 17. Measured channel loss for vertically polarized antennas at 1.2 m and 2.0 m. 37

Figure 18. Measured channel loss for horizontally polarized antennas at 1.2 m and 2.0 m. 38

Figure 19. Additional foliage loss based on measurements for vertically and horizontally polarized antennas at 1.2 m and 2.0 m. 40

Figure 20. Additional foliage loss based on measurement symbols versus LS curves for foliage with vertical and horizontally polarized antennas at 1.2 m and 2.0 m. 41

Figure 21. Estimated attenuation constant due to foliage as a function of distance. 42
Figure 22. Plane-Earth loss versus distance and transmitting and receiving antenna height. 44
Figure 23. Comparison between losses for vertically polarized antennas at 1.2 m with existing empirical models and the new empirical model....46
Figure 24. Comparison between losses for horizontally polarized antennas at 1.2 m with existing empirical model and the new empirical model. 46
Figure 25. Comparison between losses for vertically polarized antennas at 2.0 m with existing empirical models and the new empirical model....47
Figure 26. Comparison between losses for horizontally polarized antennas at 2.0 m with existing empirical model and the new empirical model. 47
Figure 27. Comparison of the empirical model versus measured data for vertically polarized antennas in foliage at 1.2 m. 49
Figure 28. Comparison of the empirical model versus measured data for horizontally polarized antennas in foliage at 1.2 m. 49
Figure 29. Comparison of the analytical model results versus measured data for vertically polarized antennas in foliage at 2.0 m. 50
Figure 30. Comparison of the analytical model results versus measured data for horizontally polarized antennas in foliage at 2.0 m. 50
Figure 31. Comparison between vertical and horizontal polarization at 1.2 m....51
Figure 32. Comparison between vertical and horizontal polarization at 2.0 m....51
Figure 33. Deterministic propagation model....53
Figure 34. Attenuation constant for combinations of relative permittivity and conductivity....54
Figure 35. Excess attenuation loss for vertically polarized antenna at 1.2 m immersed in lossy slab with $\hat{\alpha} = 0.0845$ Np/m 56
Figure 36. Excess attenuation loss for horizontally polarized antenna at 1.2 m immersed in lossy slab with $\hat{\alpha} = 0.0845$ Np/m 56
Figure 37. Excess attenuation loss for vertically polarized antenna at 2.0 m immersed in lossy slab with $\hat{\alpha} = 0.0845$ Np/m 57
Figure 38. Excess attenuation loss for horizontally polarized antenna at 2.0 m immersed in lossy slab with $\hat{\alpha} = 0.0845$ Np/m 57
Figure 39. Comparison of the analytical model versus measured data for vertically polarized antennas in foliage at 1.2 m. 58

Figure 40. Comparison of the analytical model versus measured data for horizontally polarized antennas in foliage at 1.2 m. 59
Figure 41. Comparison of the analytical model versus measured data for vertically polarized antennas in foliage at 2.0 m. 59
Figure 42. Comparison of the analytical model versus measured data for horizontally polarized antennas in foliage at 2.0 m. 60
Figure 43. Forest dielectric block constructed in FEKO. 62
Figure 44. S-parameter result for the selected dimensions of the dipole antenna 63
Figure 45. Comparison of results generated by FEKO versus measured data for vertically polarized antennas in foliage at 1.2 m. 65
Figure 46. Comparison of results generated by FEKO versus measured data for horizontally polarized antennas in foliage at 1.2 m. 66
Figure 47. Comparison of results generated by FEKO versus measured data for vertically polarized antennas in foliage at 2.0 m. 66
Figure 48. Comparison of results generated by FEKO versus measured data for horizontally polarized antennas in foliage at 2.0 m. 67

THIS PAGE INTENTIONALLY LEFT BLANK

LIST OF TABLES

Table 1. Transmitting and receiving antenna specifications (from [28]).....29

Table 2. Measured channel loss values (dB) at 5.0 m, 15.0 m, 25.0 m, and 35.0 m. 38

Table 3. Relative measured channel loss between 5.0 m and 15.0 m, 15.0 m and 25.0 m, and 25.0 m and 35.0 m.....39

Table 4. Fitting parameters and RMSE values for measurements in foliage with vertical and horizontal polarization at 1.2 m and 2.0 m. 42

Table 5. RMSEs for fitting of measurements to different empirical models.....48

Table 6. Electrical properties of the simulated media.....62

THIS PAGE INTENTIONALLY LEFT BLANK

LIST OF ACRONYMS AND ABBREVIATIONS

CAD	Computer Aided Design
CEM	Computational Electromagnetics
DG	Dual Gradient
EM	Electromagnetics
EFIE	Electric Field Integral Equation
GO	Geometrical Optics
ITU	International Telecommunication Union
LOS	Line of Sight
MA	Maximum attenuation
MED	Modified Exponential Decay
MFIE	Magnetic Field Integral Equation
MLFMM	Multilevel Fast Multipole Method
MOM	Method-of-Moments
NZG	Non-Zero Gradient
PO	Physical Optics
PGF	Path Gain Factor
RF	Radio Frequency
RMS	Root Mean Square
RMSE	Root Mean Square Error
UHF	Ultra High Frequency
VHF	Very High Frequency
VNA	Vector Network Analyzer
WSN	Wireless Sensor Network

THIS PAGE INTENTIONALLY LEFT BLANK

ACKNOWLEDGMENTS

Foremost, I would like to thank Professor David Jenn for his guidance, continuous support and patience on the development of this thesis.

To Professor Phillip Pace, for his valuable time and willingness as a second reader of this thesis.

To my family, because of their constant encouragement that drove me where I am today, I will always be grateful for that.

And to all those that one way or another, made of this journey a great experience, by helping me to survive two years of graduate school in a foreign country without going mentally insane.

THIS PAGE INTENTIONALLY LEFT BLANK

I. INTRODUCTION

A. COMPLEXITY OF A FORESTED ENVIRONMENT CHANNEL

A substantially large portion of the surface of the Earth is covered by vegetation. Because of this, the necessity to design efficient communications systems and wireless sensor networks (WSN) that operate in forested environments for military, industrial and scientific applications is crucial [1]. Characterization of radio waves propagating through foliage is a challenging task due to the complexity and random characteristics of the channel. Establishing propagation loss prediction models plays a significant role in the research of this field [2].

Attenuation introduced by vegetation elements can be compared to the reduction of the propagated radio signals in buildings and urban areas. The diversity of operational contexts for radio wave propagation through foliage is infinite, ranging from tall, dense canopy forests to open, low, sparse canopy woodlands [3], as illustrated in Figure 1. The number of physical scenarios is unlimited; therefore, arriving at a universally valid model is practically impossible.

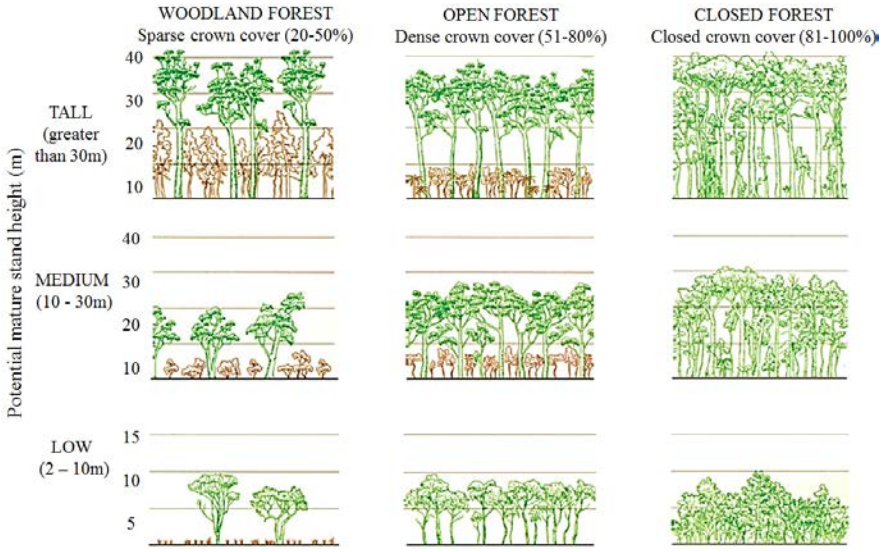

Figure 1. Different characteristics of forested environments (after [3]).

Additional effects on propagation are induced by factors such as diffraction, reflection, and multiple scattering by the ground, trunks, branches, and leaves. These propagation mechanisms severely degrade the signal quality and reduce the link distance. Depolarization and media absorption determine the attenuation of the transmitted signal and the eventual breakdown of the link at a specific distance. Also, in spite of having a detailed understanding of the properties of the channels, other non-controllable factors (e.g., wind, rain, temperature, and leaf state) have a noticeable influence on the received signal.

On a clear line-of-sight (LOS) path, where there are no obstacles or ground reflections between the transmitting and receiving stations, the signal is determined primarily by the direct signal. For cases in which the receiver is located inside a forested area, the multiple scattering mechanisms and ground reflections result in path loss with strong small-scale fluctuations with depth fading; thus, the overall signal is the superposition of the remaining LOS signal and the signals reflected from the forest-ground interface and forest-air interface. These effects are depicted in Figure 2.

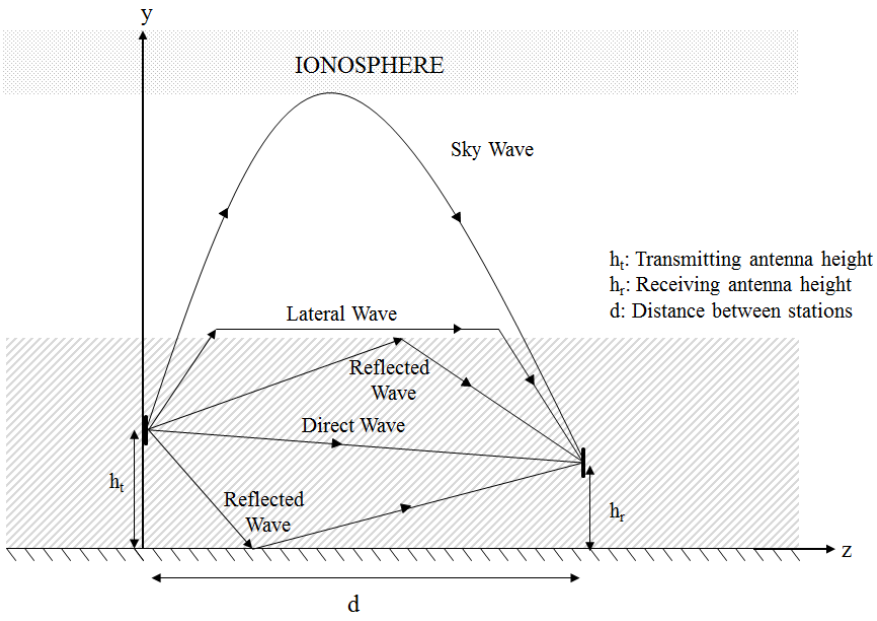

Figure 2. Simplified forest model and waves contributions (after [4]).

The attenuation is dependent on the ratio between wavelength and physical dimension of vegetation elements. When operating at low frequencies, the scattering body is much smaller than the wavelength. Conversely, medium-sized irregularities represented by tree elements have an impact on signal fading. Spread-spectrum communications and the desire for high data rates demand higher operational frequencies and broader spectral occupancy. Increasing the frequency leads to a greater decay rate because of a larger interaction between the incident signal and the vegetation.

Four widely accepted propagation modes by which the transmitted signal can reach the receiver station are described in [4]: surface-wave propagation, sky-wave propagation, lateral-wave propagation, and direct-wave propagation through foliage. These are shown in Figure 2. These modes were investigated for very high frequency (VHF) ranges [4]. It was shown that for higher frequencies, the direct wave is the predominant signal. The ground-forest interface was disregarded in [4], implying the contribution generated at this interface is negligible compared to the other propagation modes. Reflected waves resulting from the ground-forest interface constitute an important component in near-ground propagation in the ultra high frequency (UHF) band.

A near-ground scenario is the situation where the transmitting and receiving antennas are at low heights (0.5 to 3.0 m above ground) and the heights are small compared to the range. An increasing interest has emerged for loss prediction for near-ground channels, primarily because of its usefulness in military applications, such as communications between dismounted troops or battlefield WSNs [5].

B. EXISTING APPROACHES

Analytical approaches based on layered models have been proposed in order to simplify the problem [6], [7]. The number of layers mainly depends on the vegetation characteristics of the channel (leaf density, trunk diameter, canopy thickness, etc.) as shown in Figure 3. These models consider homogeneous and isotropic dielectric slabs placed over a conducting Earth, where each slab represents a different section of the forest. Although more accurate results are obtained with a greater number of layers, the implementation of theoretical models is complicated.

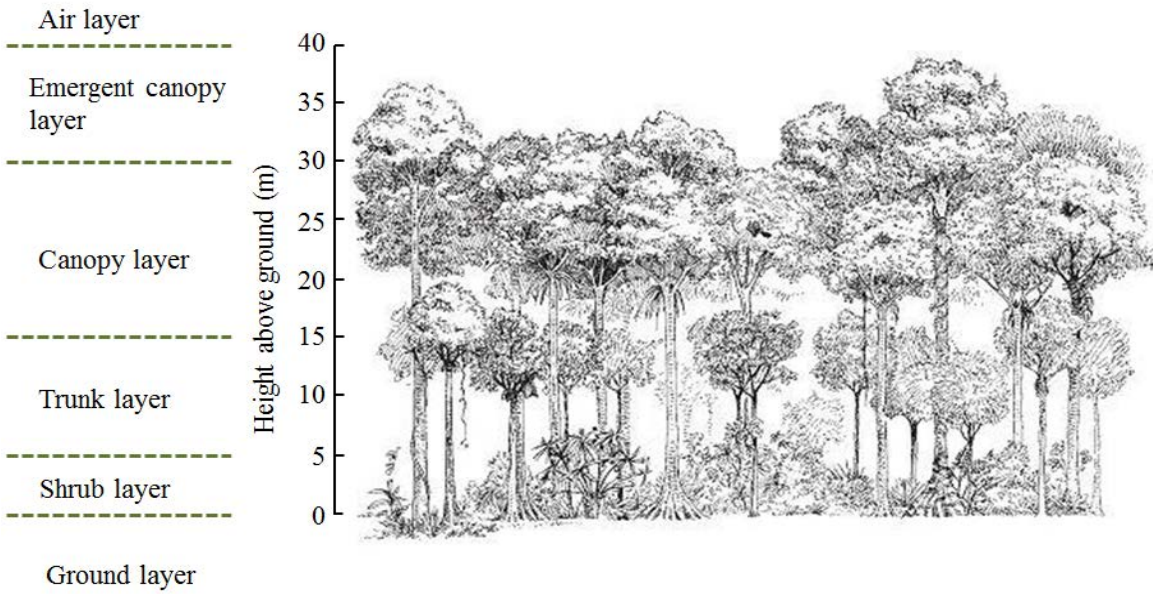

Figure 3. Stratified model of tropical rainforest (after [2]).

For years, research was focused on investigating the actual propagation loss due to foliage, which resulted in empirical models based on measured data. The main advantage of these models is their simplicity and straight-forward applicability. Still, their drawback is that each model is only related to a particular data set, which is not applicable to a general use.

Attempting to compensate for the shortcomings of the empirical models, information from both on-site geometries and attenuation properties from measurements were combined, leading into semi-empirical models [8]. These models tend to oversimplify both approaches and have very limited regions of validity.

Computational models based on the Monte Carlo simulations of propagation through stochastic distributed realistic looking fractal trees provides another alternative approach to traditional scattering models [9]. Although high accuracy can be accomplished with this approach, it requires detailed and extensive physical and structural data (i.e., tree density and height, trunk, branches and leaves dimensions, etc.) and requires significant computational resources. Even obtaining a high level of precision, stochastic models are only valid for loss prediction where the measurements were taken.

With ever-improving computational electromagnetics (CEM) methods and software, finding new tools to address an implementation that may be complicated with other approaches can now be set up with relative ease. Typically, for CEM approaches, channel dynamics—which vary over time—are ignored.

C. THESIS OBJECTIVE

Vegetation is an unavoidable feature for most outdoor wireless channels. Several prediction models were examined in the past in order to estimate propagation loss in foliage but have only yielded limited results, leaving a research gap that must be filled so that a more comprehensive solution can be achieved. The wide scope of models makes it difficult to choose a reliable, accurate approach for a new scenario.

One objective herein is to evaluate alternative models to predict the excess attenuation suffered by radio wave signals propagating through foliage. A major constraint on designing a model is the limited availability of experimental data. New experimental field measurements were conducted in an operational context that has not been previously investigated. Measurements were performed over an electrically large forested environment at 2.4 GHz.

A new model was computed through regression curves fitted to the measured data. This model was compared against the predictions of existing applicable empirical models. Dependence of propagation loss on trees was determined for the scenario, and electromagnetic (EM) foliage parameters were retrieved. A deterministic model based on forest macroscopic geometry was formulated. A simulation model was generated with CEM software using these parameters. These three models were compared against the experimental field measurements.

D. THESIS OUTLINE

This thesis is arranged into seven chapters and is organized as follows.

In Chapter I, general background about radio wave propagation through foliage served as an introduction to the topic, and the objectives of this thesis were provided.

In Chapter II, a review of empirical models is presented, and their situational applicability is explained in detail. Additionally, propagation mechanisms for analytical models are addressed, as well as other criteria that have to be considered on the development of the models.

In Chapter III, the experiment design and the measurement campaign are described. Measured data is processed and presented.

In Chapter IV, the experimental measurements are analyzed and EM parameters are estimated. The excess loss due to vegetation is computed and used to establish an empirical model, which is compared with several existing empirical models and field measurements.

In Chapter V, parameters extracted from measured data are used to establish a deterministic model based on a three-layered analytical model.

In Chapter VI, information gathered from the empirical and analytical models is employed to set up a simulation model.

In Chapter VII, a summary of findings and conclusions are presented, along with suggestions of some possible future work.

II. MODELING PARAMETERS, TECHNIQUES AND METHODOLOGY

A. ELECTRICAL PROPERTIES OF THE MEDIA

The basic electromagnetic properties for any media that influence the radio wave propagation characteristics are the permittivity ε, the permeability μ and the conductivity σ [10]. Permittivity and permeability of lossless materials that are different from a vacuum can be expressed as real quantities

$$\varepsilon = \varepsilon_0 \varepsilon_r \tag{1}$$

and

$$\mu = \mu_0 \mu_r \tag{2}$$

where $\varepsilon_0 = 8.853 \times 10^{-12}$ F/m is the permittivity of free-space and $\mu_0 = 4\pi \times 10^{-7}$ H/m is the permeability of free-space. The variable ε_r is called the relative dielectric constant or relative permittivity. The variable μ_r is known as the relative permeability. For non-magnetic materials, μ_r is set to one, and the resulting value for Eq. (2) is assumed to be equal to μ_0.

For time-harmonic fields, phasors can be used, and the permittivity can be expressed as a complex value ε_c. It consists of two terms, a real component ε' and an imaginary component ε'' [11]; hence, a complex version of Eq. (1) may be written as

$$\varepsilon_c = \varepsilon' - j\varepsilon'' = \varepsilon - j\frac{\sigma}{\omega} = \varepsilon_0 \varepsilon_r - j\frac{\sigma}{\omega} = \varepsilon_{rc}\varepsilon_0 \tag{3}$$

where $\omega = 2\pi f$ is the angular frequency in rad/s for a frequency f, and $j = \sqrt{-1}$. A $e^{+j\omega t}$ time convention is used. The imaginary part in Eq. (3) is associated with losses due to absorption and attenuation. The magnitude of these losses is dependent on the conductive behavior of the material and the propagating wave frequency.

For waves propagating in a homogeneous, isotropic, lossy dielectric, Maxwell's equations in the phasor domain relate the $\vec{\mathbf{E}}$ and $\vec{\mathbf{H}}$ fields [11] as

$$\nabla \times \vec{\mathbf{E}} = -j\omega\mu\vec{\mathbf{H}}, \tag{4}$$

and

$$\nabla \times \vec{\mathbf{H}} = \sigma\vec{\mathbf{E}} + j\omega\varepsilon_c\vec{\mathbf{E}} \ , \tag{5}$$

respectively. Wave equations can be derived from Eq. (4) and Eq. (5), yielding [11]

$$\nabla^2\vec{\mathbf{E}} + \omega^2\mu\varepsilon\left[1 - j\frac{\sigma}{\omega\varepsilon}\right]\vec{\mathbf{E}} = 0, \tag{6}$$

and

$$\nabla^2\vec{\mathbf{H}} + \omega^2\mu\varepsilon\left[1 - j\frac{\sigma}{\omega\varepsilon}\right]\vec{\mathbf{H}} = 0 \ . \tag{7}$$

The complex wavenumber k_c concept can be introduced as

$$k_c = \omega\sqrt{\mu\varepsilon_c} = k_0\sqrt{\varepsilon_{rc}} \tag{8}$$

where $k_0 = \sqrt{\varepsilon_0\mu_0}$ is the wavenumber for free-space.

Define the propagation constant as

$$\gamma = \sqrt{-\omega^2\mu\varepsilon\left[1 - j\frac{\sigma}{\omega\varepsilon}\right]} = \sqrt{-\omega^2\mu\varepsilon_c} = j\omega\sqrt{\mu\varepsilon_c} = jk_c \ . \tag{9}$$

The propagation constant γ is used to describe the effect a medium has on a signal traveling through it and can be separated into two components as

$$\gamma = \alpha + j\beta \tag{10}$$

where α is the attenuation constant in Np/m and β is the phase constant in rad/m. The attenuation constant determines the amplitude decay per unit distance in the medium. The phase constant determines the change in phase per unit distance in the medium. Solving for the real and imaginary components of Eq. (9), we express α and β as

$$\alpha = \omega\left\{\frac{\mu\varepsilon}{2}\left[\sqrt{1+\left(\frac{\sigma}{\omega\varepsilon}\right)^2}-1\right]\right\}^{\frac{1}{2}} \tag{11}$$

and

$$\beta = \omega\left\{\frac{\mu\varepsilon}{2}\left[\sqrt{1+\left(\frac{\sigma}{\omega\varepsilon}\right)^2}+1\right]\right\}^{\frac{1}{2}}, \tag{12}$$

respectively. Having established the propagation constant, we can rewrite Eq. (6) and Eq. (7) as

$$\nabla^2\vec{\mathbf{E}} - \gamma^2\vec{\mathbf{E}} = 0 \tag{13}$$

and

$$\nabla^2\vec{\mathbf{H}} - \gamma^2\vec{\mathbf{H}} = 0, \tag{14}$$

respectively.

Simplifying the wave equation for a uniform plane wave with electric field $\vec{\mathbf{E}} = \hat{\mathbf{x}}\vec{E}_x(z)$ propagating in the z-direction, we get from Eq. (13)

$$\frac{\partial^2\vec{E}_x(z)}{\partial z^2} - \gamma^2\vec{E}_x(z) = 0\ . \tag{15}$$

The solution to Eq. (15) consists of two waves (each of them traveling in opposite directions along the *z*-plane) resulting in

$$\vec{E}_x(z) = E_{x0}^{+}e^{-\gamma z} + E_{x0}^{-}e^{\gamma z} = E_{x0}^{+}e^{-\alpha z}e^{-j\beta z} + E_{x0}^{-}e^{\alpha z}e^{j\beta z} \tag{16}$$

where $E_{x0}^{\pm}$ is the initial electric field. Considering only the component traveling in the $+z$-direction, we have the magnitude of the electric field

$$\left|\vec{E}_x(z)\right| = \left|E_{x0}e^{-\alpha z}e^{-j\beta z}\right| = \left|E_{x0}\right|e^{-\alpha z}\ . \tag{17}$$

The propagation distance required to attenuate the electric field by a factor of e^{-1} is called the skin depth δ_s of the medium and is given by

$$\delta_s = \frac{1}{\alpha} \ . \tag{18}$$

For a wave amplitude $\left|E_x\left(z=\delta_s\right)\right| = \left|E_{x0}\right| e^{-1}$, the distance δ_s indicates how far the wave can penetrate into a conductive medium. Attenuation of the electric field with distance is depicted in Figure 4. Generally, because attenuation is related to frequency and conductivity by Eq. (11), lower frequency waves can penetrate further into lossy media [10].

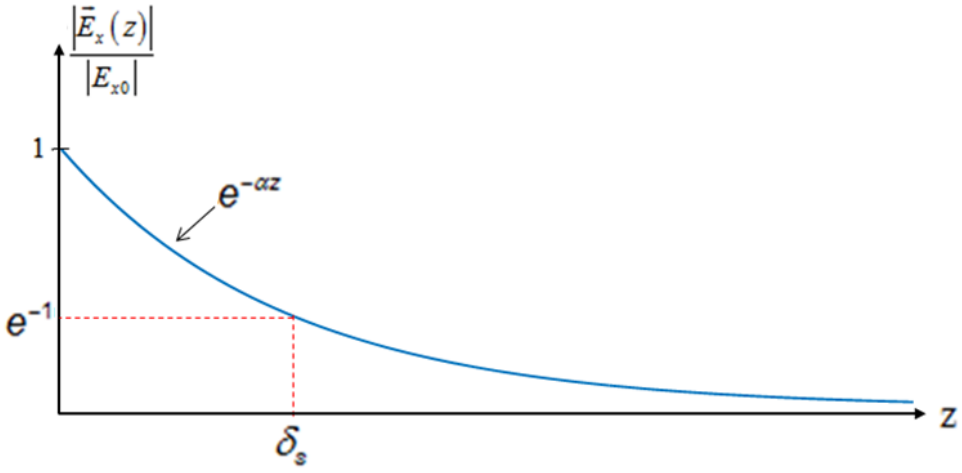

Figure 4. Attenuation of the magnitude of $E_x\left(z\right)$ as a function of distance z, (after [11]).

A foliage medium comprises many randomly distributed discrete scatterers, so it is far from being considered a homogeneous and isotropic medium; however, the media can be approximated by mean effective parameters [12], allowing the forest to be represented as a uniform continuous dielectric block on a macroscopic scale. The effective parameters are mainly dependent on the frequency, vegetation distribution, and foliage density.

Given that the forest is a non-magnetic medium ($\mu = \mu_o$), the permittivity ε and conductivity σ are critical parameters for model development. Unfortunately, very few actual measurements for these parameters are available. A good understanding of the dielectric properties of vegetation is vital for extraction of useful information.

Approaches to determine these parameters are related to the utilization of the inverse method [12] in order to estimate foliage attenuation and electrical properties. The method consists of collecting data experimentally to establish quantitative values for effects on radio waves due to vegetation, such as transmission losses over distance and attenuation factors. Effective permittivity and conductivity are estimated by fitting a forest slab model to the measured data. Parameters may only apply to the locations and conditions in which the measurements were taken.

It was observed in [13] that measurements over a wide variety of forested media suggested that the effective relative permittivity could fluctuate between 1.01 and 1.5. The effective conductivity takes on values between 10^{-5} S/m and 10^{-3} S/m. For all scenarios, it was noticed that a larger permittivity is associated with a larger conductivity; thus, the lower limits and upper limits are expected to occur together. Dense foliage environments result in larger values for dielectric parameters; therefore, there is more attenuation.

An important aspect to highlight is the frequency dependence of the electrical properties of the media. Larger values for electrical properties accompany operation at higher frequencies because the wavelength is more likely to interact with the dissipative nature of vegetation elements. Parameters estimated in [13] were obtained for frequencies from 2 to 800 MHz. Presumably, these values increase with higher frequencies.

Another consideration for radio wave propagation is the properties of the ground. For sufficiently short distances, a reflected wave generated by the ground-forest layer reaches the receiving point and is possibly a principal contributor to the overall field. The values of relative permittivity and conductivity for various types of ground for different conditions are found in the International Telecommunication Union (ITU) ITU-R Recommendation 527–3 [14].

B. ANALYTICAL METHODS FOR PATH MODELING AND LOSS PREDICTION

In [4], a model incorporating the forest features was proposed, where a lossy slab layer represents the forested environment. The model is acceptable for VHF ranges because the forest features are small compared to the wavelength, and the medium can be considered as homogeneous.

The postulated approach was shown to be valid because it demonstrates a good agreement with the experimental results obtained in [13], where the measurements were collected from a rainforest with 30.0 m tall trees with an average tree spacing of 5.0 m. It is reasonable to assume other frequency ranges may also be valid for different forest conditions.

For this research, main contributions to received fields were attributed to the direct wave, ground-reflected wave, wave reflected from the forest-air interface, sky-wave and lateral-wave components, as shown in Figure 5.

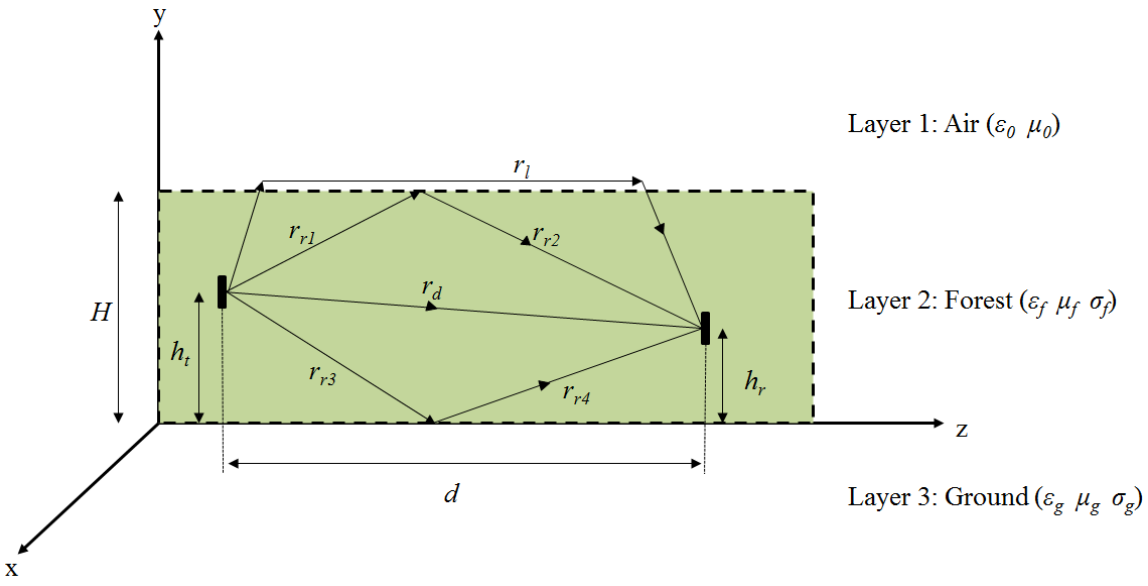

Figure 5. Propagation mechanisms in a three-layer model of the forest, (after [4]).

The geometrical optics (GO) fields consist of the direct and reflected rays. Each of these contributions are predominant within a certain range of parameters. It was noticed that the sky wave has predominance only for long distances (longer than one-hop or over 100 km) and frequencies below 10.0 MHz and is negligible otherwise. Ground effects are often not influential on the overall field. This is especially true if high gain antennas are used.

Direct waves, reflected waves from the ground-forest and forest-air interfaces, and a lateral are depicted in Figure 5, where the dissipative slab represents the forested medium with mean height *H*. The transmitting antenna is positioned at a height h_t and separated from the receiving antenna (at height h_r) by a distance *d*. The subscripts *f* and *g* refer to the forest and ground electrical properties, respectively.

First, consider the GO contributions consisting of the direct ray and the reflected ray produced by the forest-air interface. The electric field E_{Canopy} representing the combination of these two rays for a short dipole with constant current [4] can be expressed as

$$E_{Canopy} = E_{d-Canopy} + E_{r-Canopy} = 60 I_0 l \left(g_d \frac{e^{-\gamma r_d}}{r_d} + g_r \frac{e^{-\gamma (r_{r1} + r_{r2})}}{(r_{r1} + r_{r2})} \right) \tag{19}$$

where $E_{d-Canopy}$ is the direct component of the field propagating in canopy, $E_{r-Canopy}$ is the reflected component field propagating in canopy, I_0 is the transmitting antenna current, l is the short dipole length, r_d is the length of the directed wave path, g_d and g_r are normalized functions of the antenna patterns, r_{r1} is the distance between the transmitting antenna to the reflecting point on the forest-air interface, and r_{r2} is the distance between the reflecting point on the forest-air interface and the receiving antenna. For the scenarios considered herein, g_d is set to be equal to g_r, and both of them are equal to one.

Potentially, a lateral wave is formed at the reflection at the forest-air interface, leaking energy back into the forest layer as it travels tangentially along the boundary and eventually reaches the receiving antenna. The wave propagating along the forest-air boundary encounters less vegetation, and the path attenuation is significantly reduced. Furthermore, the surface wave does not spread isotropically, which also reduces loss. The incident radiation suffers total reflection at the forest-air interface at the critical angle θ_c [4], given by

$$\theta_c = \sin^{-1}\left(\frac{1}{\sqrt{\varepsilon_c}}\right). \tag{20}$$

The electric field for the lateral wave E_{Lat} is expressed as [4]

$$E_{Lat} = \frac{60 I_0 l}{\varepsilon_{rc} - 1}\left(\frac{e^{-jk_0\left[\left(r_l\sqrt{\sqrt{\varepsilon_{rc}}-1}\right)\left(2H-h_t-h_r\right)\right]}}{r_l^2}\right) \tag{21}$$

where r_l is the distance traveled by the lateral wave, h_t is the transmitting antenna height and h_r the receiving antenna height.

As the frequency increases, the lateral wave propagating along the top of a sufficiently large forest depth is no longer a valid assumption [15]. The roughness of the tree-air interface attenuates the wave because the non-uniform dimensions of the tree tops tend to be significantly larger than the wavelength. Given that the lateral wave is substantially attenuated, the vegetation elements generating multiple scattering represent a major contribution to the radio wave propagating over the forest depth.

Next, consider the possibility of a ground reflected wave. For cases where the transmitting antenna illuminates both the receiving antenna and the ground surface, the received field is comprised of the direct ray and the specular reflection from the ground. A situation assuming distances where Earth curvature is negligible (i.e., flat Earth), is illustrated in Figure 6.

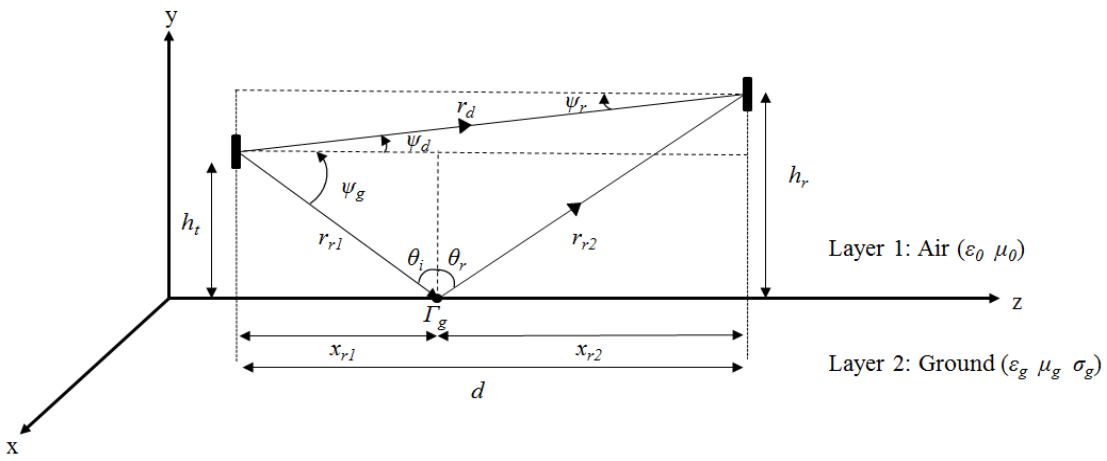

Figure 6. Propagation mechanisms for ground reflection problem (after [10]).

In Figure 6, ψ_d is the angle described by the LOS formed by the transmitting and receiving antennas, ψ_g is the angle described by trajectory between the transmitting antenna and the reflecting point on the ground, θ_i is the angle of incidence of the ground-reflected ray, θ_r is the angle formed by the reflected ray, x_{r1} is the distance between the projection of the transmitting antenna on the ground to the point of reflection, and x_{r2} is the distance between the point of reflection and the projection of the receiving antenna on the ground. By Snell's law of reflection [11] the reflected angle θ_r is equal to the incident angle θ_r. Multiple scenarios with various locations of transmitting and receiving antennas were considered in [15]. Some cases did account for the reflected wave from ground, though only for instances in which foliage was not the medium of propagation.

The electric field E_d corresponding to the direct path, the first term in Eq. (19) with $r_d \approx d$ in the denominator, is given by

$$E_d = \frac{E}{d} e^{-\gamma r_d} \cos\psi_d \tag{22}$$

where E is a constant. For the reflected ray, a critical factor is the reflection coefficient of the ground, because the strength of the reflected ray depends on this value. The

reflection coefficient is related to the intrinsic impedance of the ground η_g, the angle-of-incidence θ_i and the angle-of-transmission θ_t, given, respectively, by

$$\theta_i = \tan^{-1}\left(\frac{h_t}{x_{r1}}\right), \tag{23}$$

and

$$\theta_t = \sin^{-1}\left(\frac{\sin\theta_i}{\sqrt{\mu_r \varepsilon_{cr}}}\right). \tag{24}$$

The reflection coefficient for vertical polarization is given by [11]

$$\Gamma_{\|} = \Gamma_V = \frac{\eta_g \cos\theta_t - \eta_0 \cos\theta_i}{\eta_g \cos\theta_t + \eta_0 \cos\theta_i}\ . \tag{25}$$

The reflection coefficient for horizontal polarization is expressed as [11]

$$\Gamma_{\perp} = \Gamma_H = \frac{\eta_g \cos\theta_i - \eta_0 \cos\theta_t}{\eta_g \cos\theta_t + \eta_0 \cos\theta_i} \tag{26}$$

where η_0 is the intrinsic impedance of the air equal to $120\pi\ \Omega$.

Knowing the electrical properties of the ground, we find its intrinsic impedance from

$$\eta_g = \sqrt{\frac{\mu_0 \mu_g}{\varepsilon_0 \varepsilon_{cg}}}\ . \tag{27}$$

The reflection coefficient is used to express the reflected fields from the ground $E_{r_{gnd}}$ with $r_{r1} + r_{r2} \approx d$ in the denominator of Eq. (19) as

$$E_{r_{gnd}} = \frac{E}{d}\Gamma_g e^{-\gamma(r_{r1}+r_{r2})}\cos\psi_r \tag{28}$$

where Γ_g is taken as either $\Gamma_{\|}$ or $\Gamma_{\perp}$ depending on the polarization of the antenna. By combining E_d and $E_{r_{gnd}}$, we obtain the total field

$$E_{tot_{gnd}} = E_d + E_{r_{gnd}} = \frac{E}{d}\left(e^{-\gamma r_d}\cos\psi_d + \Gamma_g e^{-\gamma(r_{r1}+r_{r2})}\cos\psi_r\right). \quad (29)$$

For conditions where $\psi_d \approx \psi_r$, Eq. (29) can be rewritten as

$$E_{tot} = \frac{E\cos\psi_d}{d}\left[e^{-\gamma r_d} + \Gamma_g e^{-\gamma(r_{r1}+r_{r2})}\right]. \quad (30)$$

Note that the phase factors of γr_d and $\gamma(r_{r1}+r_{r2})$ can differ by millions of radians for small wavelengths [10].

A good measure of the propagation effect on field strength is the path gain factor (PGF), the factor in brackets in Eq. (30):

$$F = e^{-\gamma r_d} + \Gamma_g e^{-\gamma(r_{r1}+r_{r2})} \quad (31)$$

where F represents the PGF. Note that F gives the field strength relative to a free-space LOS. For a free-space propagation case, where $\alpha = 0$, Eq. (31) becomes

$$F = e^{-\beta r_d} + \Gamma_g e^{-\beta(r_{r1}+r_{r2})} = e^{-\gamma r_d}\left(1+\Gamma_g e^{-\beta\left[(r_{r1}+r_{r2})-r_d\right]}\right) = 1+\Gamma_g e^{-\beta\Delta R} \quad (32)$$

where $\Delta R = \left(r_{r1}+r_{r2}\right) - r_d$ is the path difference. If the forest layer is considered as a continuous lossy dielectric medium, the attenuation affecting the radio waves is present in the PGF equation that modifies the propagation pattern. The direct wave component and the ground-reflected wave component described in Eq. (32) are modified separately because the decay rate is proportional to the distance travelled by each wave.

Given the forest layer is bounded by a highly conductive ground, the principal factors affecting the propagation mechanisms are the conduction losses induced by the presence of vegetation and the presence of the ground-forest interface. The path inside the forest layer of any reflected wave is longer than the path of the direct wave; thus, the ground-reflected wave experiences more attenuation. The modified PGF that includes attenuation is expressed as

$$\left|F\right| = \left|e^{-\alpha r_d} + \Gamma_g e^{-j\beta\Delta R} e^{-\alpha(r_{r1}+r_{r2})}\right|. \quad (33)$$

The PGF is related to the field at the receiver and takes on values $0 \le |F| \le 2$. The excess attenuation loss in dB L_{att} is derived from Eq. (33) as

$$L_{att}(dB) = -20\log_{10}\left(\left|e^{-\alpha r_d} + \Gamma_g e^{-j\beta\Delta R} e^{-\alpha(r_{r1}+r_{r2})}\right|\right) = -20\log_{10}\left(|F|\right) . \quad (34)$$

When it comes to describe losses, it is more convenient to express them as positive quantities, hence the minus sign in Eq. (34). Given that the constructive and destructive interferences between the direct wave and the ground-reflected wave give alternate maxima and minima in the overall excess attenuation loss, "negative losses" in dB may be expected in small regions immediately next to the transmitter.

The function of the PGF of Eq. (33) is to modify the received power by accounting the propagation effects in a free-space scenario. For a basic case of LOS propagation through free-space [16], the received power P_r is given by

$$P_r = P_t G_t G_r \left(\frac{\lambda}{4\pi d}\right)^2 \quad (35)$$

where P_t is the transmitted power in Watts, G_t is the gain of the transmitting antenna, G_r is the gain of the receiving antenna, and λ is the wavelength of the correspondent operational frequency. The received power computed by Eq. (35) is known as the Friis transmission formula [17]. The inverted term $\left(4\pi d^2/\lambda\right)$ of Eq. (35) is called the free-space path loss L_0 [18] and represents the free-space reduction in signal strength at the antenna terminals separated by a distance d. Note that the free-space path loss is frequency dependent; however, Eq. (35) does not account for other losses in the link. To correct this, terms that represent the effect of losses due to transmission medium and system losses (i.e., impedance mismatch, polarization mismatch and connector losses) must be included. Taking the system losses L_{sys} into consideration transforms Eq. (35) into

$$P_r = \frac{P_t G_t G_r}{L_{sys}} \left(\frac{\lambda}{4\pi d}\right)^2 . \quad (36)$$

Note that the system loss factor is in the denominator, and $L_{sys} \geq 1$, inferring it reduces the received power.

At this point, it is convenient to restate Eq. (36) in its logarithmic form

$$P_r\left(dBW\right) = 10\log_{10} P_t + 10\log_{10} G_t + 10\log_{10} G_r + 20\log_{10}\left(\frac{\lambda}{4\pi d}\right) - 10\log_{10} L_{sys} \text{ .(37)}$$

In this expression, the notation $P_r\left(dBW\right)$ indicates that the received power is specified in decibels relative to 1 W. In decibel notation, and recalling the definition of the free-space path loss L_0, Eq. (37) can be written as

$$P_r\left(dBW\right) = P_t\left(dBW\right) + G_t\left(dB\right) + G_r\left(dB\right) - L_0\left(dB\right) - L_{sys}\left(dB\right) \text{ .} \quad (38)$$

The PGF in Eq. (33) can be added to the logarithmic form of the modified Friis transmission formula. The received power becomes

$$P_r\left(dBW\right) = P_t\left(dBW\right) + G_t\left(dB\right) + G_r\left(dB\right) - L_0\left(dB\right) - L_{sys}\left(dB\right) + 20\log_{10}\left|F\right| \text{ .} \quad (39)$$

Finally, using the definition of the excess attenuation loss L_{att} of Eq. (34) in Eq. (36), we can rewrite Eq. (39) as

$$P_r\left(dBW\right) = P_t\left(dBW\right) + G_t\left(dB\right) + G_r\left(dB\right) - L_0\left(dB\right) - L_{sys}\left(dB\right) - L_{att}\left(dB\right). \quad (40)$$

C. EMPIRICAL METHOD FOR PATH MODELING AND LOSS PREDICTION

The improvement of the analytical approaches is dependent on how accurately the environment can be modeled in order to get a high level of precision by adding more variables and geometry parameters [19]. Unfortunately, this can only be accomplished using advanced numerical analysis methods to obtain a solution for the complex mathematical formulations, and significant computational resources are required [20]. Also, advanced analytical models are strongly dependent on data from direct measurements for evaluation, modification and validation. The data depend on features of site-specific scenarios. Based on the ensemble of experimental measurements, empirical approaches may be developed through regression techniques. Even though they do not

account for the physics involved, they aim to provide an estimate of excess attenuation (over and above the attenuation caused by free-space LOS propagation); therefore, empirical models give a fair understanding of the quantitative losses because they are based on actual data.

The main advantage of empirical methods is the simplicity of the mathematical expression that describes them. Just because a model is simpler, it does not strictly mean that it is doomed to failure. It is far more practical to verify a simple model rather than understanding a more complex one for which critical inputs are not available.

Several empirical models for radiowave propagation through foliage have been proposed. The models discussed in this section are those that apply to the operating frequency of interest that are used in subsequent measurements. Empirical models can be classified into two main categories: modified exponential decay (MED) and maximum attenuation (MA). MA models, such as the non-zero gradient (NZG) model and the dual-gradient (DG) model are actually semi-empirical models because the attenuation gradient varies with distance, considering the effect of geometry on their formulation [8]. Although the frequency-of-interest herein is valid for the valid frequency ranges of the semi-empirical models, they are not discussed in this section.

1. Weissberger Model

In [21], an empirical propagation model was proposed by Weissberger as a modification of the exponential decay (EXD) due to its various limitations. Originally called the modified exponential decay (MED) model, it was developed by using experimental data obtained from different forested environments in the United States over a frequency range of 230 MHz and 95 GHz. It is applicable in contexts where radiowave propagation is likely to occur through dense, dry, in-leaf trees found in temperate climates. Both transmitting and receiving antennas are assumed to be immersed in foliage, so radiation travels through vegetation rather than being diffracted at the forest-air interface. Even if the model is suggested for short distances, plane-Earth losses were not taken into account. The Weissberger model formulation is given as

$$L_W\left(dB\right)=\begin{cases}1.33\,f_{GHz}^{0.284}d^{0.588}, & 14\text{ m}\le d\le 400\text{ m}\\ 0.45\,f_{GHz}^{0.284}d, & 0\text{ m}\ \le\ d\ \le\ 14\text{ m}\end{cases} \tag{41}$$

where L_W is the vegetation loss in dB, f_{GHz} is the frequency in GHz, and d is the vegetation depth in meters between the transmitting antenna and the observation point.

2. International Telecommunication Union – Recommendation (ITU-R)

In 1986, The ITU developed a model from measurements mainly in the UHF band [22]. The model is suitable for vegetation depths less than 400.0 m for frequencies between 200 MHz and 95 GHz. The measurement setup involved a grove of trees separating the transmitting and the receiving antenna, so the majority of the signal propagated through foliage. The ITU-R model was proposed as

$$L_{ITU-R}\left(dB\right)=0.2\,f_{MHz}^{0.3}d^{0.6} \tag{42}$$

where L_{ITU-R} is the vegetation loss in dB and f_{MHz} is the frequency in MHz.

3. Fitted ITU-R (FITU-R) Model

After optimizing the three numerical values of the ITU-R model based on experimental measurements at 11.2 GHz and 20 GHz for foliage depths no thicker than 120.0 m in-leaf and out-of-leaf, Al-Nuaimi and Stephens [23] developed the FITU-R model. The model is recommended for use up to 40 GHz. The FITU-R model was compared with the ITU-R model based on fitting several measurements sets using a least-squares error fit, yielding a smallest root-mean square error (RMSE). The FITU-R model is expressed as

$$L_{FITU-R}\left(dB\right)=\begin{cases}0.37\,f_{MHz}^{0.18}d^{0.59}, & \text{out-of-leaf}\\ 0.39\,f_{MHz}^{0.39}d^{0.25}, & \text{in-leaf}\end{cases} \tag{43}$$

where L_{FITU-R} is the vegetation loss in dB.

4. Lateral ITU-R (LITU-R) Model

In [24], Meng modified the FITU-R to accommodate near-ground radio wave propagation for VHF and UHF bands, including the lateral wave effects. The measurements for the model development were set over large tropical plantations in Singapore at 240 and 700 MHz. The LITU-R model is given by

$$L_{LITU-R}\left(dB\right) = 0.48\, f_{MHz}^{0.43} d^{0.13} \tag{44}$$

where L_{LITU-R} is the vegetation loss in dB. While it is suggested to use the previously explained empirical models for short ranges, the LITU-R model has shown good agreement with experimental data up to a distance of 1.0 km.

5. COST 235 Model

The Cooperation in Science and Technology (COST) developed another model known as the COST 235 in 1996 [25]. The measurements used for the reference data of the model were obtained under different conditions for foliage such as leaf state and tree type at a frequency range between 9.6 GHz and 57.6 GHz. Applying a least-squares fit regression, the model formulation was expressed as

$$L_{COST}\left(dB\right) = \begin{cases} 26.6\, f_{MHz}^{-0.2} d^{0.5}, & \text{out-of-leaf} \\ 15.6\, f_{MHz}^{-0.009} d^{0.26}, & \text{in-leaf} \end{cases} \tag{45}$$

where L_{COST} is the vegetation loss in dB. Unlike other models, this one presents a slow and inverse dependence of attenuation on the frequency. This may affect the reliability of the model since radio wave propagation loss is expected to increase with the frequency.

6. Seville Model

In [8], Seville performed measurements on a grove of trees covering a depth of 46.0 m at 38 GHz. Experiments consisted of varying the height of a vertically-polarized antenna at trunk level, canopy level and tree-top level, each of them showing a different degree of attenuation. Semi-empirical models were generated after this investigation. The proposed prediction model is given by

$$L_S\left(dB\right) = 0.37 f_{MHz}^{0.3} d^{0.38} \tag{46}$$

where L_S is the vegetation loss in dB.

Using Eq. (41) to Eq. (46), we present a comparison of the empirical models in Figure 7. The frequency was fixed at 2.4 GHz, while the range was varied from 1.0 m to 35.0 m. All models show an increase of excess loss as vegetation depth increases.

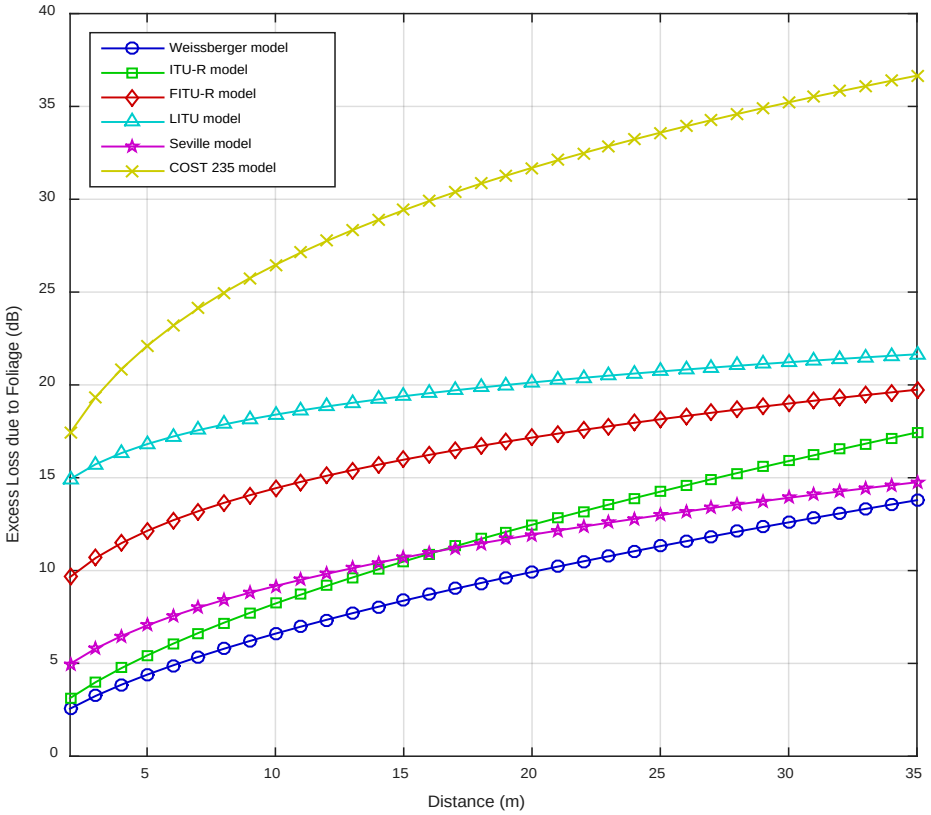

Figure 7. Excess loss versus distance at 2.4 GHz.

A second comparison of empirical models is presented in Figure 8. Distance was kept fixed at 35.0 m while frequency was varied from 1 GHz to 35 GHz. All models show an increase of excess loss due to foliage as frequency increases with the exception of the COST 235 model. In both comparisons, predicted loss differs widely for the models due to differences in the operational context upon which each one was formulated.

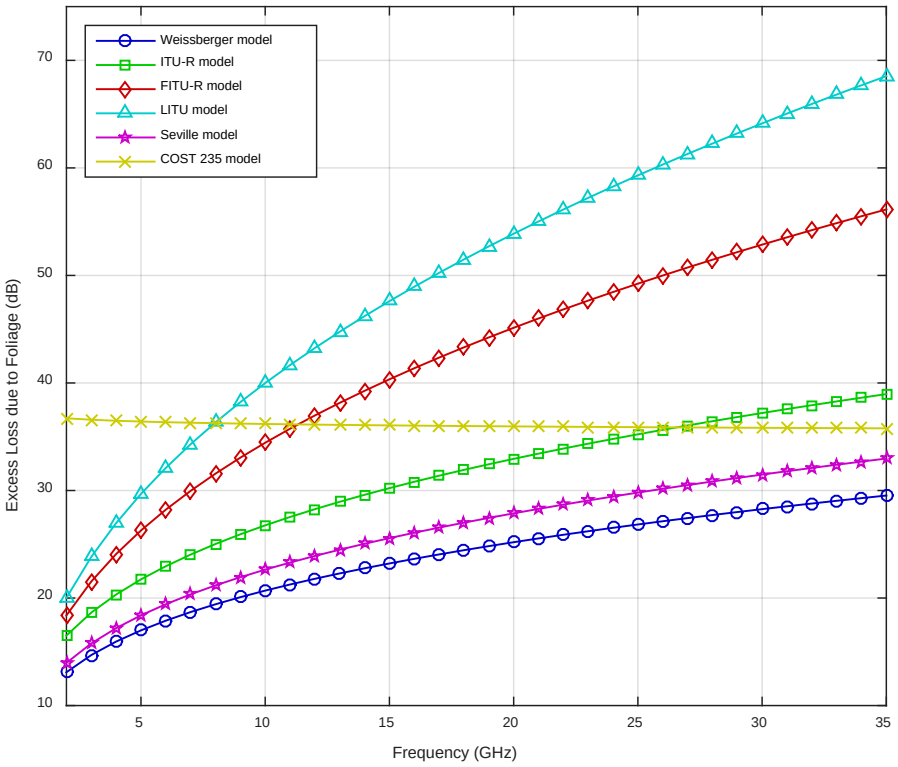

Figure 8. Excess loss versus frequency at 35.0 m foliage depth.

All the models considered are valid for relatively short link distances, where predominant propagation mechanisms are forest-air reflection, diffraction, scattering and absorption.

The actual objective of the empirical models is to estimate excess loss due to foliage for an operational context without necessarily requiring a precise knowledge of the attenuation constant of the medium. To account for this excess loss when computing the received power, the empirical model loss can be included in the modified Friis transmission formula of Eq. (38).

Basically, all the empirical models start by isolating the loss induced by foliage. This can be computed as a ratio of the received power of radio wave propagating in foliage to the received power of a LOS reference measurement, both of them with the

same atmospheric and ground conditions. This provides an additional foliage loss $L_{foliage}$ in dB that varies as a function of the distance d and is given by

$$L_{foliage}(d)(dB) = P_{r\_out-of-foliage}(d)(dBm) - P_{r\_in-foliage}(d)(dBm) \quad (47)$$

where $P_{r\_out-of-foliage}(d)$ is the received power in dBm at a distance d in a LOS scenario and $P_{r\_in-foliage}(d)$ is the received power in dBm at a distance d in a scenario where both transmitting and receiving antennas are immersed in foliage.

D. PLANE-EARTH MODEL

In [24], Meng formulated the LITU-R model, which includes effects induced by a plane-Earth because for short distances this mode needs to be considered for near-ground antennas. For this mode, if grazing incidence is assumed, $\Gamma_g = 1$, and ΔR is approximated as $2h_t h_r / d$, the PGF in free-space from Eq. (32) can be modified to

$$|F_{PE}| = \left|1 - e^{-j\beta\frac{2h_t h_r}{d}}\right| = 2\left|\sin\left(\frac{\beta h_t h_r}{d}\right)\right| . \quad (48)$$

Notice that $|F_{PE}|$ in Eq. (48) is applicable only for unobstructed propagation; hence, it does not account for signal degradation due to foliage. As a result, the plane-Earth-loss L_{PE} concept is introduced and can be derived from Eq. (48) as

$$L_{PE}(dB) = -20\log_{10}\left(2\left|\sin\left(\frac{\beta h_t h_r}{d}\right)\right|\right) = -20\log_{10}\left(|F_{PE}|\right) \quad (49)$$

where $L_{PE}(dB)$ is the plane-Earth loss expressed in dB. Again, the received power P_r is proportional to the square of $|F_{PE}|$. Including the effects of the plane-Earth-loss in the modified Friis transmission formula of Eq. (38), we get the received power

$$P_{r\_PE}(dBW) = P_t(dBW) + G_t(dB) + G_r(dB) - L_0(dB) - L_{sys}(dB) - L_{PE}(dB). \quad (50)$$

E. DEPOLARIZATION EFFECTS

Due to inconsistent geometry and media electromagnetic properties, the overall field is substantially depolarized because of the randomly oriented induced currents generated by the inhomogeneous medium [26]. The partial scattering causes energy losses in the original plane; however, this energy may appear in other planes as an undesirable component.

Given the anisotropic features of the medium, depolarization is a function of the original polarization of the emitted signal. Even though the grove is clearly a randomly distributed medium, there is a steady vertical component along the foliage geometry. For this reason, displacing either the transmitting or receiving antenna a few wavelengths away from one measurement to another may result in serious variations.

Effects of depolarization measurements in tropical rainforest were reported in [27]. For frequencies below 800 MHz, vertically polarized waves suffer more depolarization than horizontally polarized waves. Vertically oriented tree trunks dominate the absorption and scattering process. Above this frequency, both vertical and horizontal polarizations suffer a similar attenuation due to the randomly distributed, horizontally oriented branches and leaves.

III. EXPERIMENT DESIGN AND MEASUREMENT CAMPAIGN

A. EXPERIMENT SITE

The field tests were performed on Fort Ord National Monument located in the Monterey Peninsula. This is a park with a total landmass of 7,200 acres run by the Bureau of Land Management. The experimental site was selected based on criteria such as foliage density, terrain features, site accessibility, vegetation dimensions and geometry. A satellite map of the area is shown in Figure 9.

Figure 9. Experimental site satellite map.

The experiment was conducted in May, when the average temperature is 63° F and the average rainfall is 14.0 mm. The terrain is nearly flat and mainly consists of dry soil and sand that is covered by grass in some parts. The experimental site is mixed vegetation woodland with an average tree height of approximately 3.0 m. Vegetation is

irregularly distributed with sparse trees in some sections and excessively dense foliage blocks in others. Part of the foliage at the experiment site is shown in Figure 10.

Figure 10. Part of the measurement site at Fort Ord National Monument.

B. EQUIPMENT AND MEASUREMENT SETUP

The transmitter section consists of a portable computer used to power a USB-compatible signal generator LSG-402 with an operating frequency that ranges from 1.0 GHz to 4.0 GHz and generates a continuous wave RF signal up to a maximum power of +10.0 dBm (0.01 W). The advantages of this signal generator are that it is portable and does not require an additional DC supply voltage.

A carrier wave centered at 2.4 GHz was chosen as a fixed frequency. Two 1.0 m low-loss, 50-Ω coaxial cables were used to connect the signal generator to an antenna from the transmitter station. The transmitting antenna is a L-com HG2415Y radome-

enclosed Yagi antenna. It was mounted on a 2.5 m mast, where the height of the antenna height and polarization could be varied. The antenna specifications [28] are shown in Table 1. Antenna radiation patterns for both vertical and horizontal polarizations are illustrated in Figure 11. Directional antennas with high gains are used for both stations to ensure optimal power transmission through the main lobe.

Table 1. Transmitting and receiving antenna specifications (from [28]).

Electrical Specifications	
Frequency range	2.4 GHz – 2.5 GHz
Gain	14.5 dBi
Impedance	50 Ω
3 dB Beamwidth (Both planes)	30°
Polarization	Vertical (V) or Horizontal (H)
Mechanical Specifications	
Length	462 mm
Diameter	76 mm

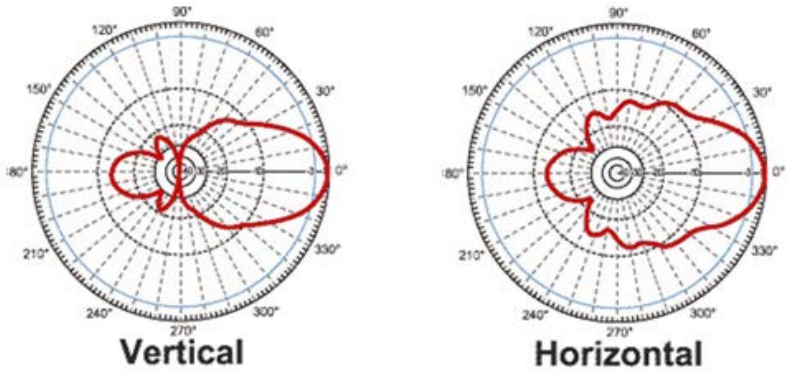

Figure 11. Transmitting and receiving antenna radiation patterns for vertical and horizontal polarizations (from [28]).

The receiver station has another HG2415Y Yagi antenna. The antenna is attached to a mast through a swivel mount, so polarization can be switched from vertical to horizontal and vice versa. Two 1.0 m low-loss, 50-Ω cables and a barrel connector were utilized to connect the antenna to an Anritsu MS2721B Spectrum Analyzer with a working frequency range of 9.0 kHz to 7.1 GHz. The equipment can detect signals with power up to +30 dBm and has a 50-Ω input impedance. During measurements, the analyzer was set to track the peak signal for a full span. A schematic diagram of the measurement setup is displayed in Figure 12.

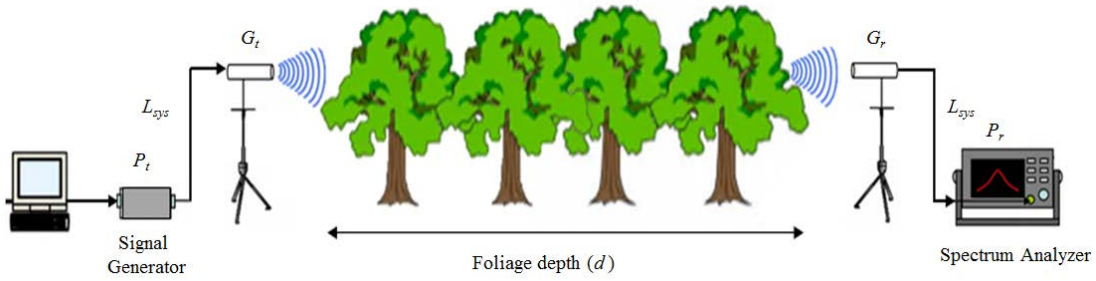

Figure 12. Schematic diagram of measurement setup (after [24]).

After verifying no signal was being radiated in the area, the noise floor established in the receiver station was -65 dBm; therefore, the depth that could be covered in foliage was subject to this limit. The signal generator was programmed to provide +10 dBm to the transmitting antenna; however, power at the output terminal of the signal generator was measured with the spectrum analyzer, finding it to actually be +6.3 dBm. This value is considered as transmitted power for future calculations.

Cable and connector losses were measured using a HP 8510C Vector Network Analyzer (VNA). A total of five cables were used to connect elements for both stations. The two, low-loss cables connecting the signal generator to the transmitting antenna add 2.08 dB of loss, while the three cables connecting the receiving antenna to the spectrum

analyzer adds 3.24 dB. Combined connection losses of 5.32 dB are addressed as system losses L_{sys} and are compensated for in the data processing phase.

Radiation regions of an antenna can be designated as either the near-field or the far-field. Antenna electromagnetic field characteristics are different depending on the distance r from the transmitting antenna. Propagation in the far field is less complicated than at short ranges, because if the distance between the transmitting antenna and the observation point is sufficiently far, the radiated field can be represented by a plane wave [10]. Three conditions must be met in order to satisfy the far-field condition [29]:

$$r > \frac{2D^2}{\lambda}$$

$$r > 5D \ , \tag{51}$$

and

$$r > 1.6\lambda$$

where D is the largest projected dimension of the transmitting antenna. Recalling $D = 0.462$ m, the far-field region starts at 3.145 m. For ranges shorter than this, the full gain of the antenna may not be realized.

Given ground and canopy reflections along the path between stations, the resultant radio waves may arrive at the receiving point with their phase shifted. A reflection point within the first Fresnel zone [10] suffers a 180° phase shift by its half-wavelength excess path and another 180° at the reflection point. Given that the reflected wave is in phase with the direct wave, the signal strength is enhanced. If the reflection occurs within the second Fresnel zone, the excess path produces a 360° phase shift. There is also a shift in phase of 180° at the reflection point. Now, the reflected signal interferes destructively with the direct one. The geometry of a Fresnel zone can be described as an ellipsoid of revolution with the direct ray as its axis. The Fresnel radius is described by

$$FZ_n = \sqrt{\frac{n\lambda d_1 d_2}{r}} \tag{52}$$

where FZ_n is the radius of the nth Fresnel zone in meters and $r = d_1 + d_2$ is the total path length. At a given point on the path, d_1 is the distance to one end of the path, and d_2 is the distance to the other end. A distance of $0.6FZ_1$ should be kept free of strong reflection points since the transmitted energy is concentrated there [10]. The largest Fresnel radius for the signal propagating through the foliage block at the selected frequency is computed with Eq. (52), resulting in 1.04 m. Antenna heights were verified to be inside the first Fresnel zone, which, considering its radius, is meant to be kept within the ground-forest interface and the forest-air interface.

A relatively dense block of foliage over a nearly flat terrain was selected for this study. The measurements were taken at two different antenna heights, 1.2 m and 2.0 m, for stations inside a foliage block. Antenna heights were chosen so a major region of the whole block was illuminated. The transmitted polarization was set for vertical and then horizontal; hence, the received field was measured for co-polarized antennas.

Throughout the measurement procedure, the transmitting antenna was kept at a fixed point. The receiving antenna was shifted to different distances along a straight line from the transmitting antenna. The receiving antenna was directed toward the transmitting station, so the maximum value of the gain was obtained. Eighteen measurement points were set along the line with slightly variable step size, covering up to a distance of 35.0 m (the noise floor limit was reached at this foliage depth). The carrier wave was sampled at one-hundred readings per second using the spectrum analyzer at each measurement position. The receiving antenna sampled long enough (15 s) at each measuring point so that an accurate value could be achieved. After the measurement was recorded, the receiving antenna was moved to the next point, and the process was repeated until all 18 recording points had been covered.

During the measurement process, we verified that the signal was propagating through foliage rather than over it, because the greatest power was obtained when the mainbeams of the antennas were pointing at each other. Shifting and rotating the antennas toward the forest-air interface of the foliage block resulted in a substantial decrease of the received power, evidencing the majority of the signal was propagated through the direct

path. Field tests were repeated in the case of unobstructed LOS, where the attenuation affecting the propagating EM field was caused only by the path length. This case forms the baseline from which foliage attenuation losses are estimated.

C. MEASUREMENT RESULTS

Results from the conducted field experiments previously described are presented in this section. Measured systems losses were subtracted from recorded power for both free-space and foliage block scenario. The measured power in free-space is compared with the measured power inside the foliage block and shown in Figure 13 to Figure 16.

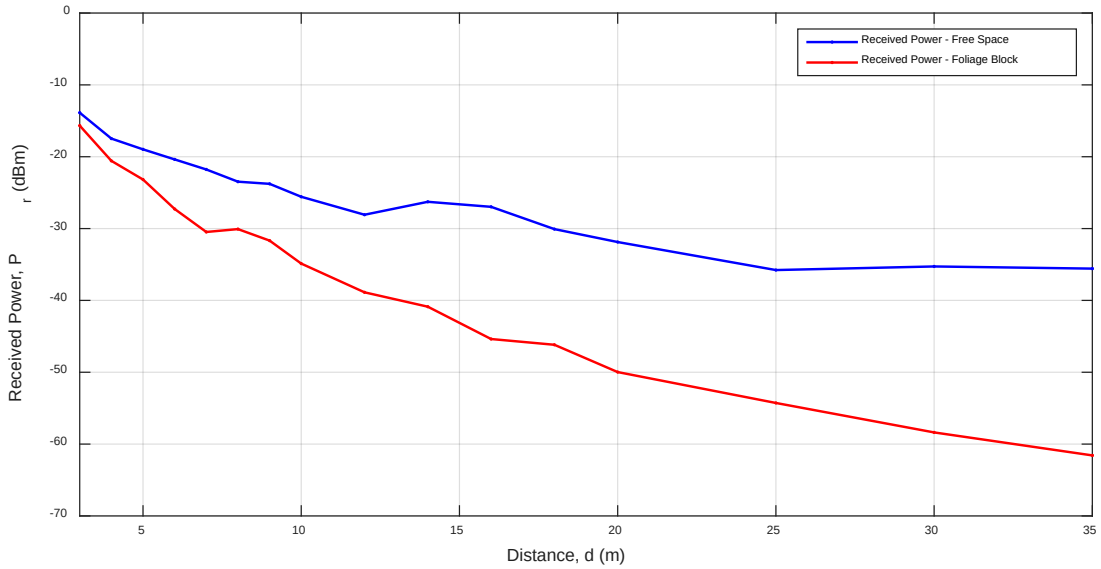

Figure 13. Measured power outside and inside the foliage block for vertically polarized antennas at 1.2 m.

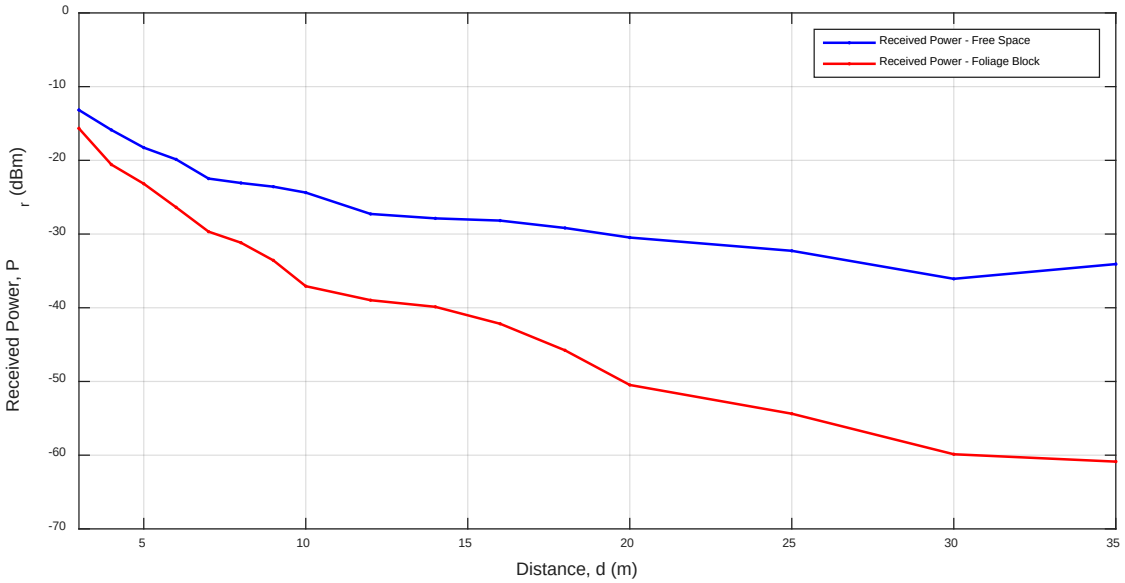

Figure 14. Measured power outside and inside the foliage block for vertically polarized antennas at 2.0 m.

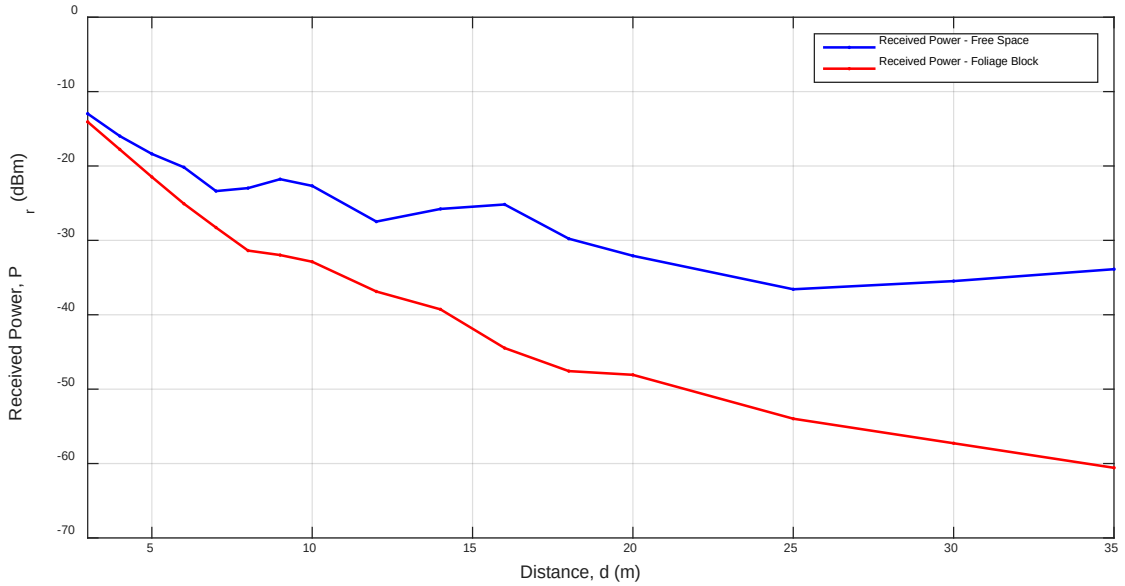

Figure 15. Measured power outside and inside the foliage block for horizontally polarized antennas at 1.2 m.

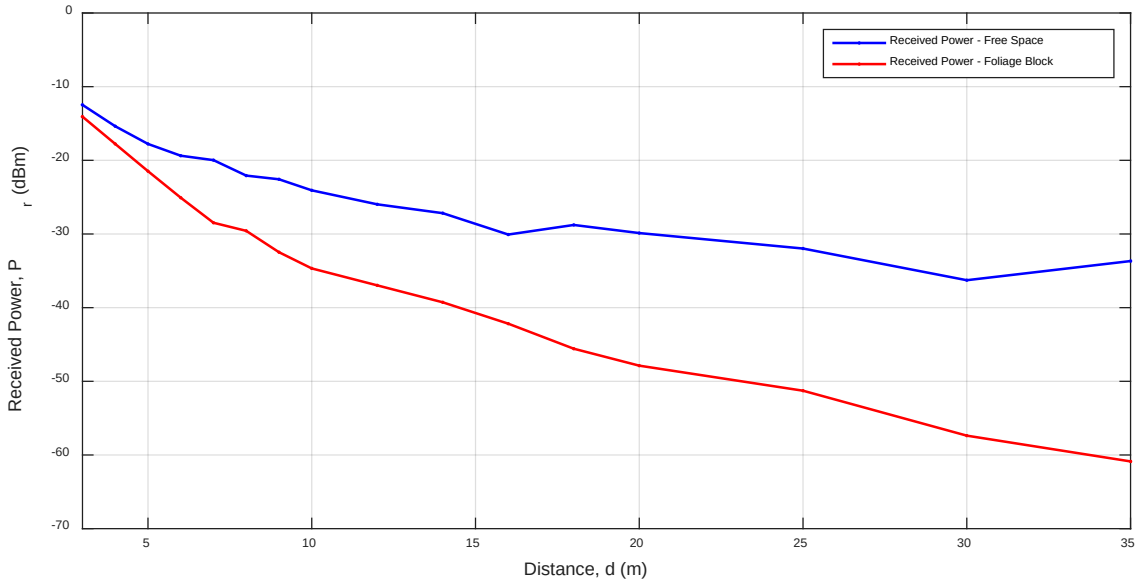

Figure 16. Measured power outside and inside the foliage block for horizontally polarized antennas at 2.0 m.

From the measured data plots, a relatively smooth curve with a constant decay is observed. It is important to point out that, in the free-space cases there are slightly noticeable signs of constructive and destructive interference on the curves, suggesting the presence of ground-reflected waves. This characteristic is not actually perceptible in forested scenarios, probably because of the consistent scattering and attenuation inside the foliage block. The performance of the models developed in the following chapters is compared with the measured data.

THIS PAGE INTENTIONALLY LEFT BLANK

IV. PATH LOSS MODELING FROM EXPERIMENTAL DATA

A. MEASUREMENTS DISCUSSION

Prior to the modeling phase, characterization of the channel was investigated. The analysis of measured data obtained by experiments conducted over short woodland paths is presented in this section. The site description and measurement details were provided in Chapter III. The measured channel loss $L_{Measured}$ in dB is calculated from

$$L_{Measured}(d)(dB) = \left(P_t(dBm) - P_r(d)(dBm)\right) - L_{sys}(dB) \ . \tag{53}$$

Notice that the transmitted power P_t remains constant, while the received power P_r varies as a function of distance, causing $L_{Measured}$ to vary with distance too. The variation of the measured channel loss with depth of vegetation was examined for different heights and polarizations. Computed losses based on measurements performed with vertically and horizontally polarized antennas immersed in foliage are shown in Figure 17 and Figure 18, respectively.

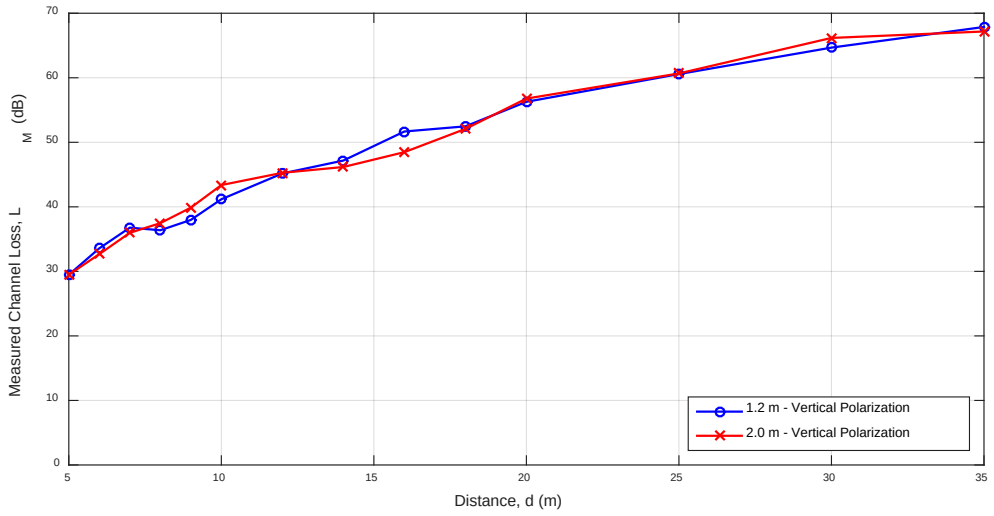

Figure 17. Measured channel loss for vertically polarized antennas at 1.2 m and 2.0 m.

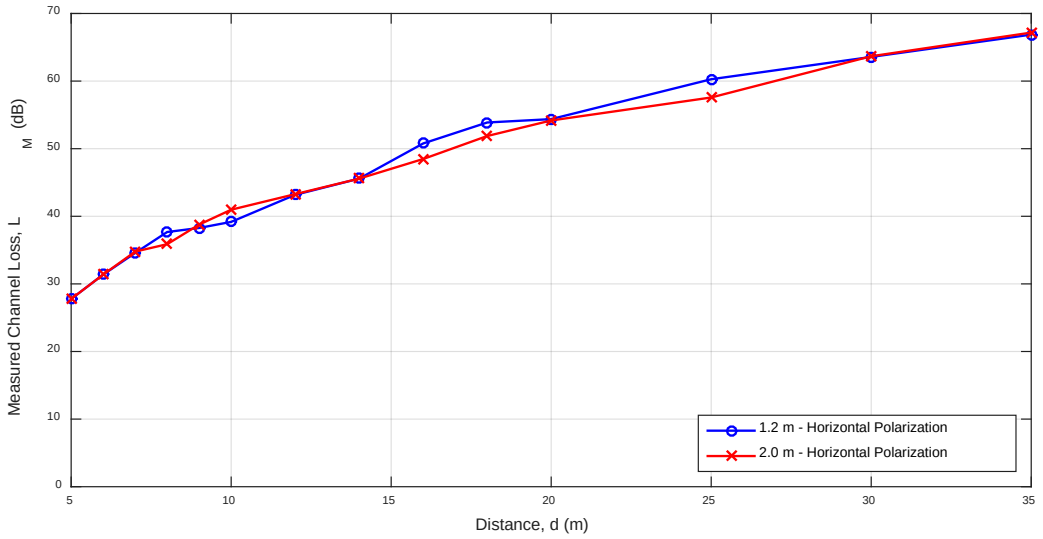

Figure 18. Measured channel loss for horizontally polarized antennas at 1.2 m and 2.0 m.

As expected, the losses increase with distance. There were no major differences in measured channel loss as a function of the antenna height for either polarization case. Four evaluation distance points (5.0 m, 15.0 m, 25.0 m, and 35.0 m) are examined for further analysis as shown in Table 2.

Table 2. Measured channel loss values (dB) at 5.0 m, 15.0 m, 25.0 m, and 35.0 m.

	5.0 m	15.0 m	25.0 m	35.0 m
V- pol at 1.2 m	29.4	54.6	61.5	67.8
H-pol at 1.2 m	27.7	53.7	65.2	66.8
V-pol at 2.0 m	29.4	49.4	60.6	67.1
H-pol at 2.0 m	27.7	51.4	59.5	66.1

An increase in loss is noted as the vegetation depth increases, but not at a constant rate. For all these distances, radio waves are partially obstructed by vegetation elements and, certainly, there is not an unobstructed propagation component. As the waves

propagate through the foliage, the reduction in attenuation may be result of re-radiation of field components from vegetation elements. At certain initial depth, a larger loss rate is expected and begins to flatten out as the foliage depth increases. The relative measured channel loss between evaluation points is presented in Table 3.

Table 3. Relative measured channel loss between 5.0 m and 15.0 m, 15.0 m and 25.0 m, and 25.0 m and 35.0 m.

	Measured channel loss between 5.0 m and 15.0 m	Measured channel loss between 15.0 m and 25.0 m	Measured channel loss between 25.0 m and 35.0 m
V- pol at 1.2 m	25.2 dB	6.9 dB	6.3 dB
H-pol at 1.2 m	26 dB	11.5 dB	1.6 dB
V-pol at 2.0 m	20 dB	11.2 dB	6.5 dB
H-pol at 2.0 m	23.7 dB	8.1 dB	6.6 dB

The large measured channel loss observed for short distances is presumed to be caused by the substantial decay of the contribution of the coherent component of the propagating signal. When the vegetation depth is larger, the coherent component does not represent the predominant contribution anymore, and the overall field is mainly influenced by scattering. The incoherent components tend to counteract the loss due to medium absorption, resulting in a lower attenuation rate. This agrees with previously reported results [8], [21], [23], [25].

B. ATTENUATION CONSTANT ESTIMATION

Weissberger proposed in [21] an approximation to obtain a differential attenuation due to foliage α_{diff} given by

$$\alpha_{diff}(d) = \frac{L_{foliage}(d)}{d} \tag{54}$$

where $L_{foliage}(d)$ is the additional foliage loss computed with (47) that estimates the value of α_{diff} for each requested distance. Even though this represents an accurate

method to estimate signal decay, it has to be performed for every sample in each data set and becomes impractical if an attenuation constant of the medium is intended to be estimated from measurements for further research. Following this premise, we computed excess loss for each data set with Eq. (47), for which the results are displayed in Figure 19. Only measurements taken in the far-field region were considered for these calculations.

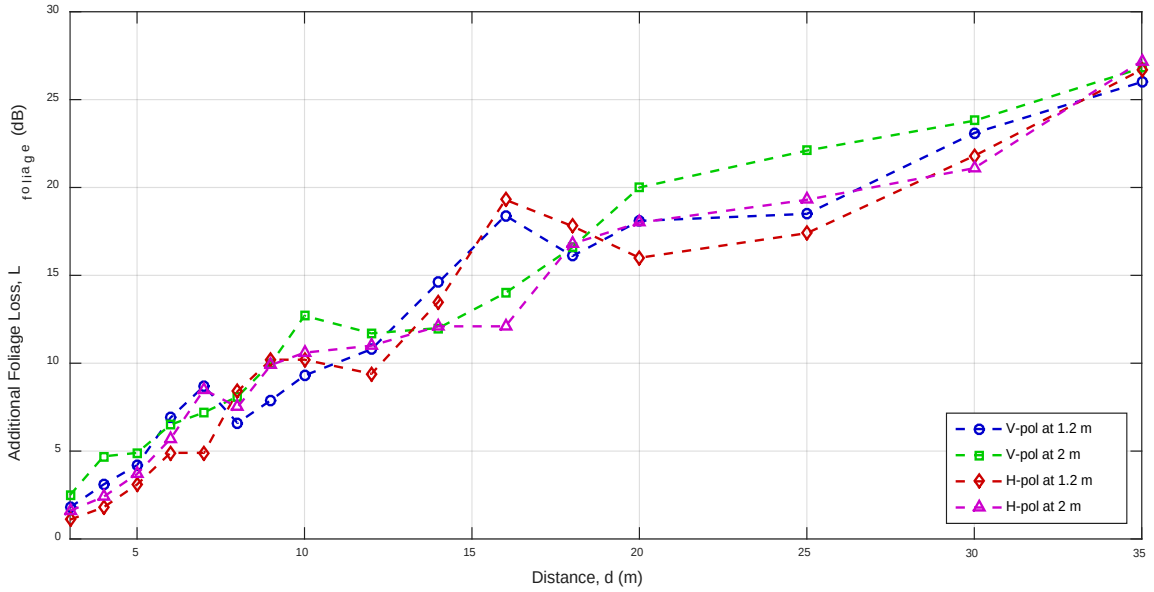

Figure 19. Additional foliage loss based on measurements for vertically and horizontally polarized antennas at 1.2 m and 2.0 m.

Based on the data, the signal power decays exponentially when the vegetation depth increases; so, an exponential function can be used for modeling the excess loss due to foliage as

$$L_{fit}\left(dB\right) = \hat{S}e^{-\hat{\alpha}d} \tag{55}$$

where L_{fit} is the predicted loss based on measured values, $\hat{S}$ is the estimated scaling parameter to be applied to the fitted curve, and $\hat{\alpha}$ is the estimated attenuation in Np/m. For each set of additional foliage loss values computed with Eq. (47), corresponding $\hat{S}$

and $\hat{\alpha}$ variables were obtained through a non-linear least-squares (LS) fit; hence, they were optimized to provide the best fit to the experimental data. Best fit curves for each excess loss data set are shown in Figure 20.

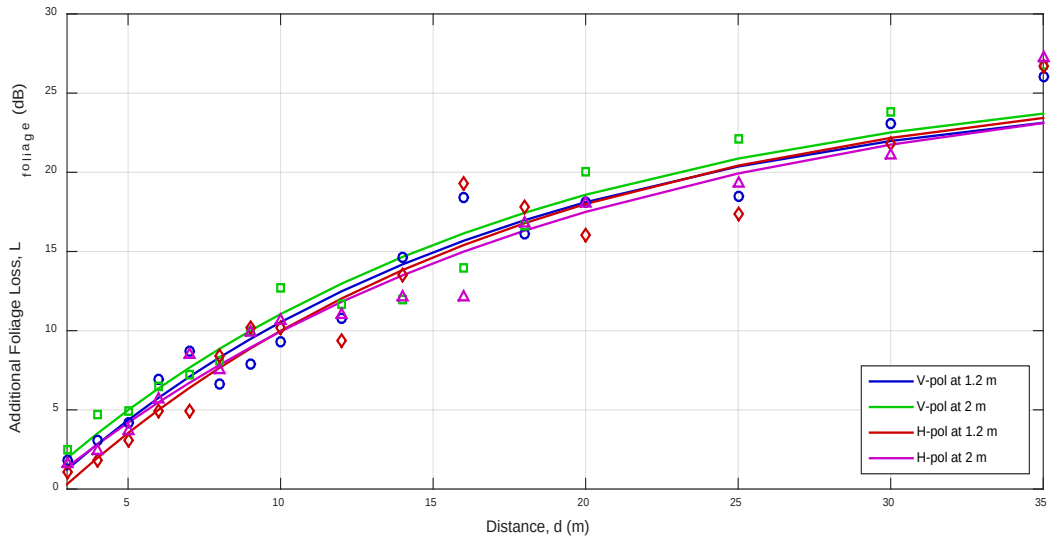

Figure 20. Additional foliage loss based on measurement symbols versus LS curves for foliage with vertical and horizontally polarized antennas at 1.2 m and 2.0 m.

Eventually, each measured data set results in different parameters, and the optimal values are verified by RMSE. RMSE, in dB, was calculated for each fitted curve model by

$$RMSE = \sqrt{\frac{\sum_{i=1}^{N}(E_i)^2}{N}} \tag{56}$$

where N is the number of measurements in each data set and E_i is the error in predicting the i^{th} measurement, computed by subtracting the measurement loss from the predicted loss. Optimal parameters with their respective RMSE are presented in Table 4.

Table 4. Fitting parameters and RMSE values for measurements in foliage with vertical and horizontal polarization at 1.2 m and 2.0 m.

	Scale parameter, $\hat{S}$	Attenuation, $\hat{\alpha}$ (Np/m)	RMSE, (dB)
V- pol at 1.2 m	– 29.0261	0.0859	0.5899
H-pol at 1.2 m	– 28.0134	0.0960	0. 4286
V-pol at 2.0 m	– 30.3065	0.0912	0.4683
H-pol at 2.0 m	– 27.8186	0.0872	0.5304

As it can be noticed from Figure 20, all of the fitted curves fall approximately in the same range, as do the estimated attenuations $\hat{\alpha}$, which is in the range of 0.0859 to 0.0960. Given this body of data, it may be possible to extract an attenuation constant for this particular medium. In order to arrive at an attenuation constant that can be used in general for conditions and locations similar to those where measurements were taken, excess losses obtained with Eq. (47) were averaged, and the result was normalized. The averaged attenuation is 0.0845 Np/m, and it was also visually determined by computing the skin depth for $e^{-1} = 0.3678$ as described in Eq. (18), resulting in 11.83 m as displayed in Figure 21.

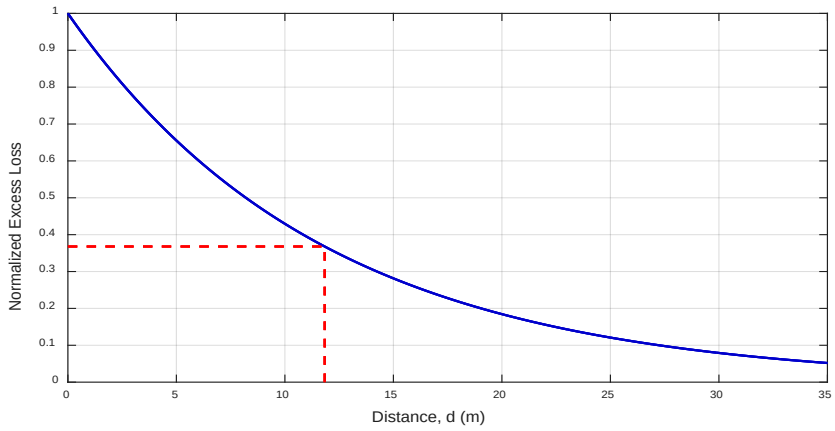

Figure 21. Estimated attenuation constant due to foliage as a function of distance.

C. EMPIRICAL PATH LOSS MODELING

Predicting the propagation loss due to foliage can be a challenging task because of the complexity that resides in the variations in operational contexts and vegetation parameters (e.g., foliage type, tree and leaf density, terrain features, measurement geometry, etc). Furthermore, characterizing each of the possible influential parameters involves a process that requires the gathering of large amounts of data. Focusing only on quantifying the additional loss due to foliage still encompasses the effects of the combined parameters.

Additional foliage loss for each measurement set was estimated in the previous section by removing the LOS loss component, and an exponential function was introduced in order to predict the decay based on these results. Even though the exponential model represents an accurate representation of the excess loss, it is only applicable when measurements are available. Additionally, even if the experimental data are combined to widen the situational coverage of the model, this may not be a reliable approach when the operational scenario changes.

One of the main drawbacks of the exponential model is the reduced number of variables playing a role in the solution. Examining the existing established empirical models, we notice that the loss induced by foliage can be represented in the form

$$L_{empirical}(dB) = A \times f^{B} \times d^{C} \tag{57}$$

where $L_{empirical}$ is the empirically-determined loss due to foliage, A is the scaling parameter, B is the frequency-dependent parameter, and C is the distance-dependent parameter. These three parameters can be determined by performing an iterative optimization process and regression techniques on the sets of measured data.

The near-ground scenario is a complex operational context because of the reflection, absorption, and obstruction occurring from the low-height vegetation and ground; therefore, it may be necessary to include the effects of near-ground antennas in the channel characterization and modeling. It is seen from the plane-Earth loss in Eq. (49) that the propagation loss is substantially reduced by increasing the height of either or both of the antennas. Examining measured channel loss displayed in Figure 17 and Figure 18,

we see that there is not a significant variation in the measured loss when the antenna height is changed.

Taking a closer look at the development of the existing empirical models, we see that the only model that considers the effects of near-ground conditions for a plane Earth is the LITU-R model [24]. Instead of using the actual plane-Earth model or its approximation for long distances ($d \gg h_t, h_r$) [17], the LITU-R model considered a fitted-ground reflection model; hence, the effects of the plane-Earth model were not fully accounted for in the LITU-R model. In order to study the influence of the antennas' heights, Eq. (49) can be analyzed as a function of distance and heights. Given that the experimental phase involved only scenarios when both transmitting and receiving antenna were at the same height, values for h_t and h_r in Eq. (49) are assumed to be the same. Isotropic antennas are assumed for this analysis. Under these conditions, plane-Earth loss computed with Eq. (49) is plotted in Figure 22.

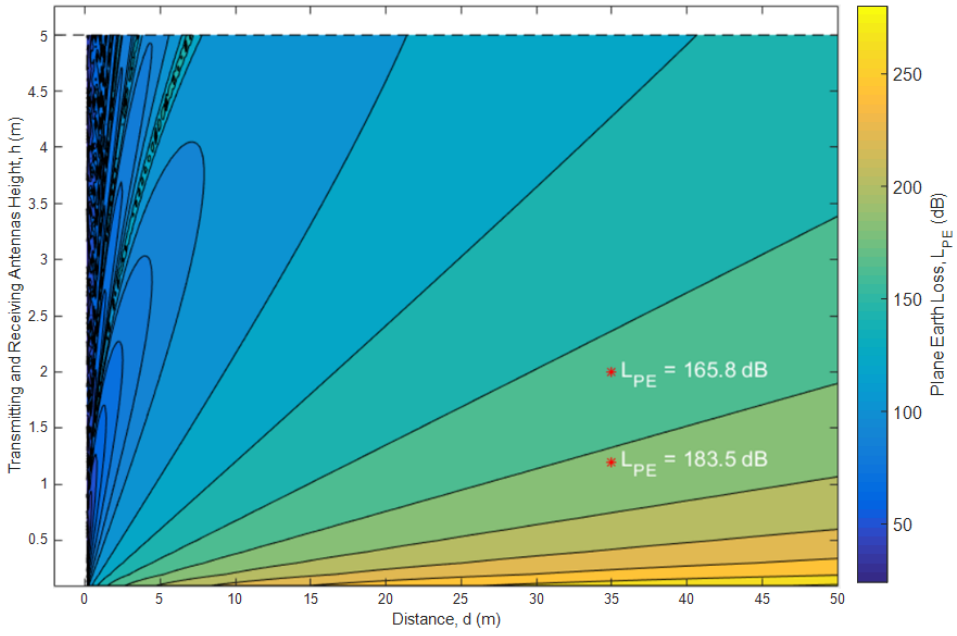

Figure 22. Plane-Earth loss versus distance and transmitting and receiving antenna height.

It is observed from Figure 22 that the predicted loss by the plane-Earth model results in significant variations depending on the antenna heights. Taking as a reference the experimental data for both polarizations, we see that measurements at different heights still had similar trends and loss levels. At one distance of interest ($d = 35.0$ m), the measured excess loss did not increase more than 1 dB when the results for 1.2 m were compared with the results for 2.0 m. Even for a free-space scenario such as the one represented in Figure 22, the plane-Earth model predicted a loss increase of 17.7 dB when the antennas were lowered 0.8 m. Notice that the loss magnitude between heights is less pronounced as the distance increases; thus, the plane-Earth model represents a valid solution for longer distances. Given the geometry characteristics of the experimental location, it may not be valid to add the plane-Earth loss to the empirical model under development.

Unlike Section IV.B, where all the experimental data was grouped together and averaged to provide a model of more general use after achieving a minimum RMSE, the parameters A, B, and C were empirically determined after achieving a minimum combined RMSE when the resulting equation was compared with all the measured data. The values estimated for A, B, and C were found to be 0.18, 0.35, and 0.59, respectively. Applying these values to Eq. (57),we get the proposed empirical model

$$L_{empirical}\left(dB\right) = 0.18\, f_{MHz}^{0.35} d^{0.59} \ . \tag{58}$$

Positive values were obtained for B and C, which infers that propagation loss increases when the frequency or the separation distance between antennas increases. The expression in Eq. (58) is proposed for the modeling of only the excess loss due to foliage. In order to evaluate the proposed model performance, additional foliage loss $L_{foliage}$ for each data set was computed with Eq. (47) and comparisons were made among the empirical models given in Eq. (41) to Eq. (46). Comparisons for different operational contexts are shown in Figure 23 to Figure 26.

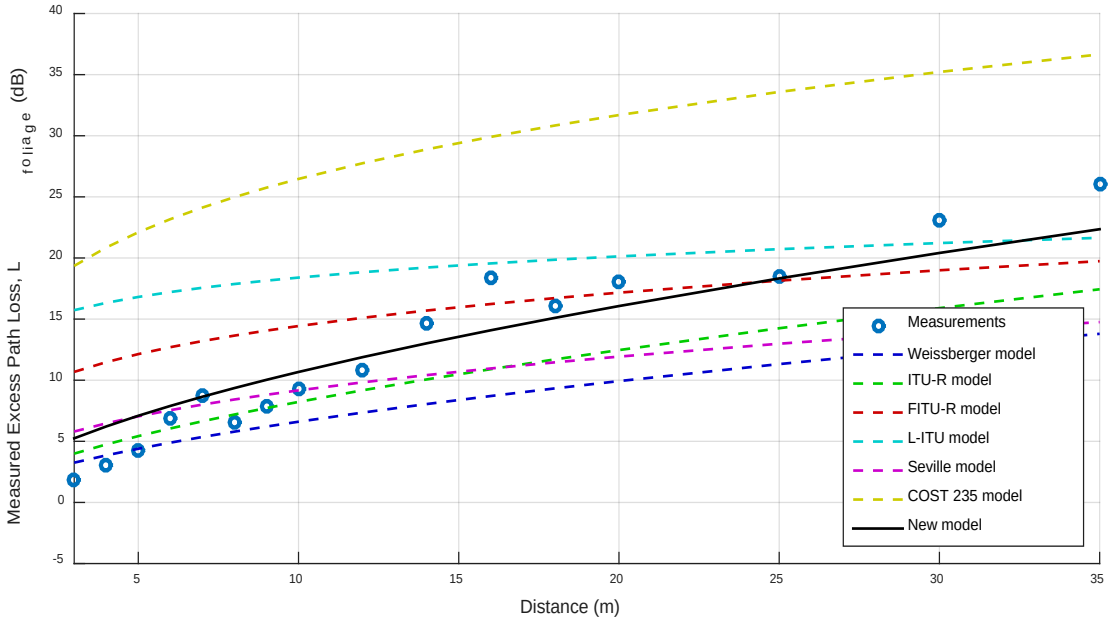

Figure 23. Comparison between losses for vertically polarized antennas at 1.2 m with existing empirical models and the new empirical model.

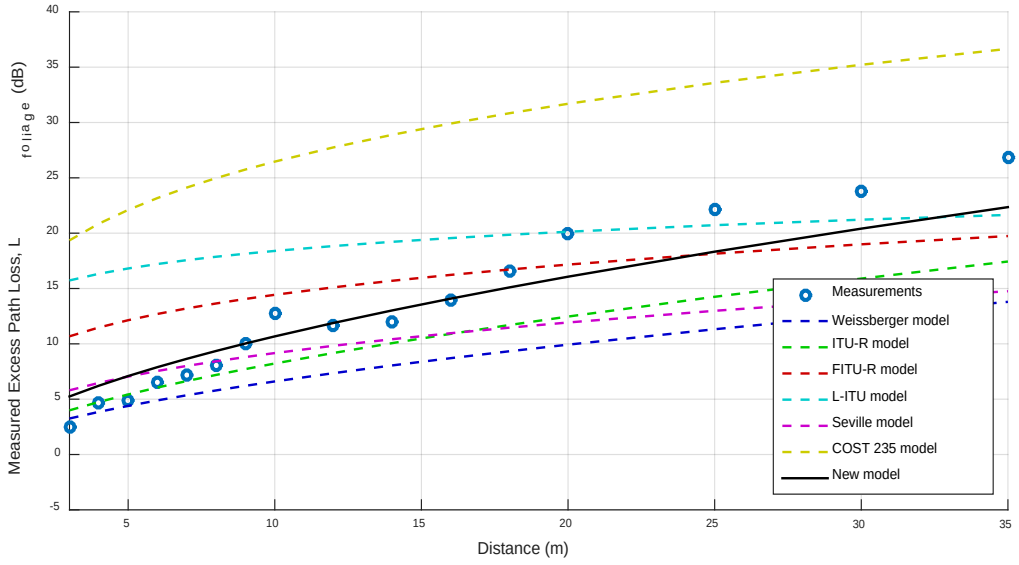

Figure 24. Comparison between losses for horizontally polarized antennas at 1.2 m with existing empirical model and the new empirical model.

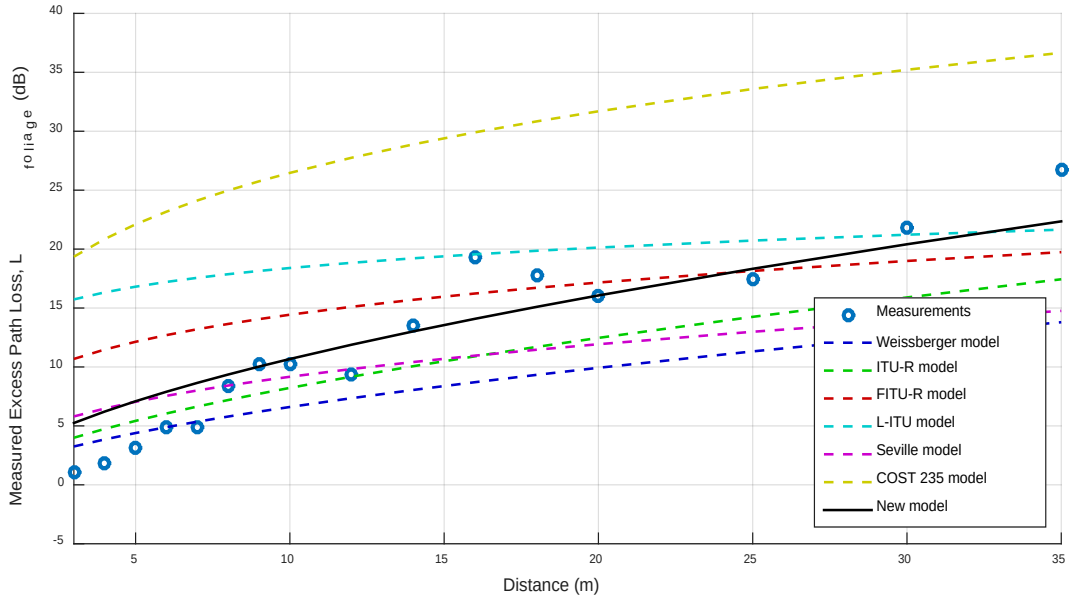

Figure 25. Comparison between losses for vertically polarized antennas at 2.0 m with existing empirical models and the new empirical model.

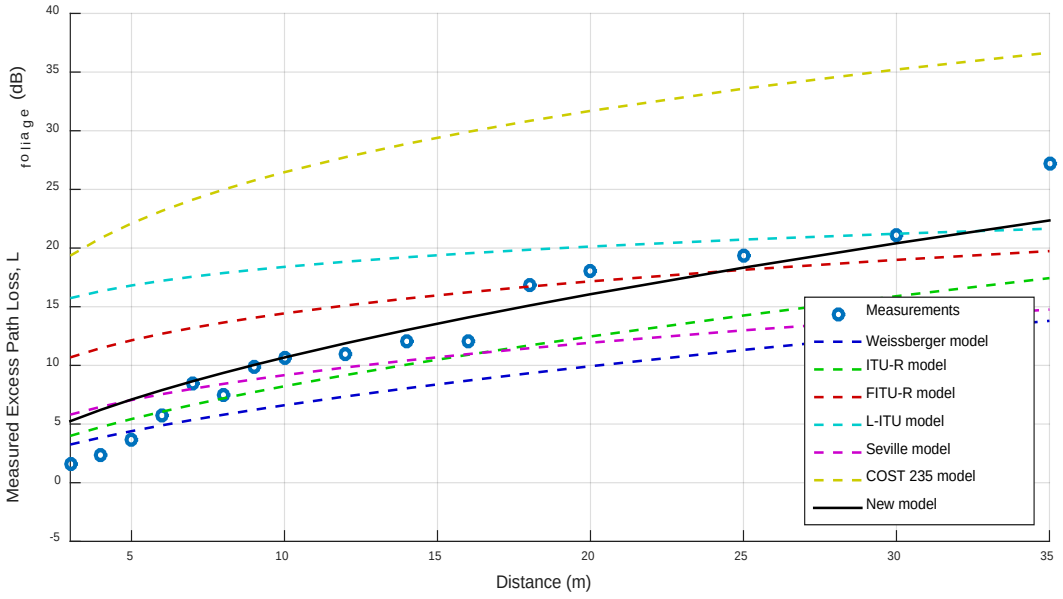

Figure 26. Comparison between losses for horizontally polarized antennas at 2.0 m with existing empirical model and the new empirical model.

Good agreement with experimental data was expected because the model is based entirely on field measurements. The performance of the proposed model was compared to the measurements and the other empirical models via RMSEs as shown in Table 5.

Table 5. RMSEs for fitting of measurements to different empirical models.

	RMSE for V-pol at 1.2 m (dB)	RMSE for H-pol at 1.2 m (dB)	RMSE for V-pol at 2.0 m (dB)	RMSE for H-pol at 2.0 m (dB)	Total RMSE (dB)
New Model	2.4105	2.3540	2.9520	2.3021	10.0186
Weissberger	6.1281	6.5765	6.0687	5.7347	24.5079
ITU-R	4.2516	4.6179	4.3363	3.8861	17.0918
FITU-R	5.3724	5.1043	5.9343	5.5112	21.9222
LITU-R	8.5175	8.0943	9.1009	8.7718	34.4844
Seville	5.0930	5.4020	5.2402	4.8107	20.5460
COST 235	15.6355	15.0469	16.1740	16.0258	62.8823

Field measurements showed a faster decay as a function of distance than the decay predicted by most of the empirical models. RMSEs between measurements and the new model were between 2.30 dB and 2.95 dB, giving smaller values than all of the RMSEs computed for the other models. The RMSE range of the new model (0.65 dB) is also the smallest among the other models' RMSEs, confirming a more variable applicability for similar scenarios.

Eventually, the predicted received power for a signal propagating in foliage can be computed by including the empirical model given by Eq. (58) in the modified Friis transmission formula of Eq. (38); therefore, the empirically determined received power $P_{r\_empirical}$ is given by

$$P_{r\_empirical}\left(dBW\right) = P_t\left(dBW\right) + G_t\left(dB\right) + G_r\left(dB\right) - L_0\left(dB\right) - L_{sys}\left(dB\right) - L_{empirical}\left(dB\right). \quad (59)$$

Comparisons of the empirically determined received power $P_{r\_empirical}$ and experimental measurements results are plotted in Figure 27 to Figure 30.

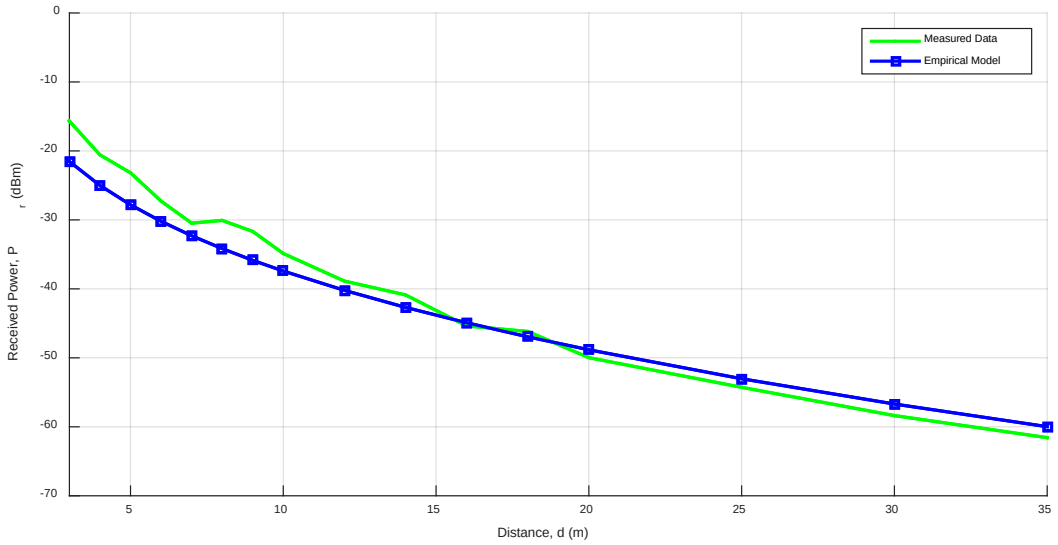

Figure 27. Comparison of the empirical model versus measured data for vertically polarized antennas in foliage at 1.2 m.

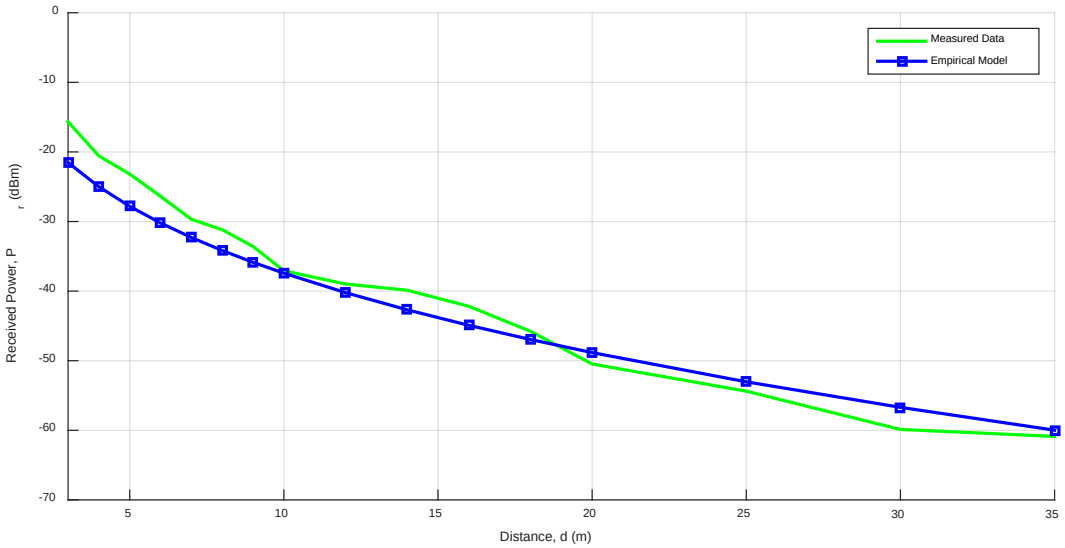

Figure 28. Comparison of the empirical model versus measured data for horizontally polarized antennas in foliage at 1.2 m.

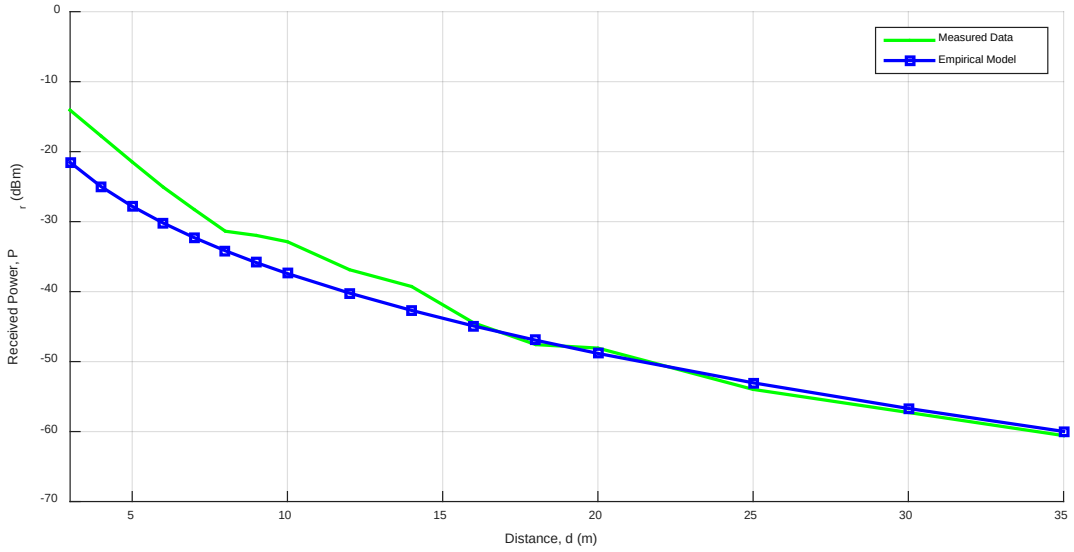

Figure 29. Comparison of the analytical model results versus measured data for vertically polarized antennas in foliage at 2.0 m.

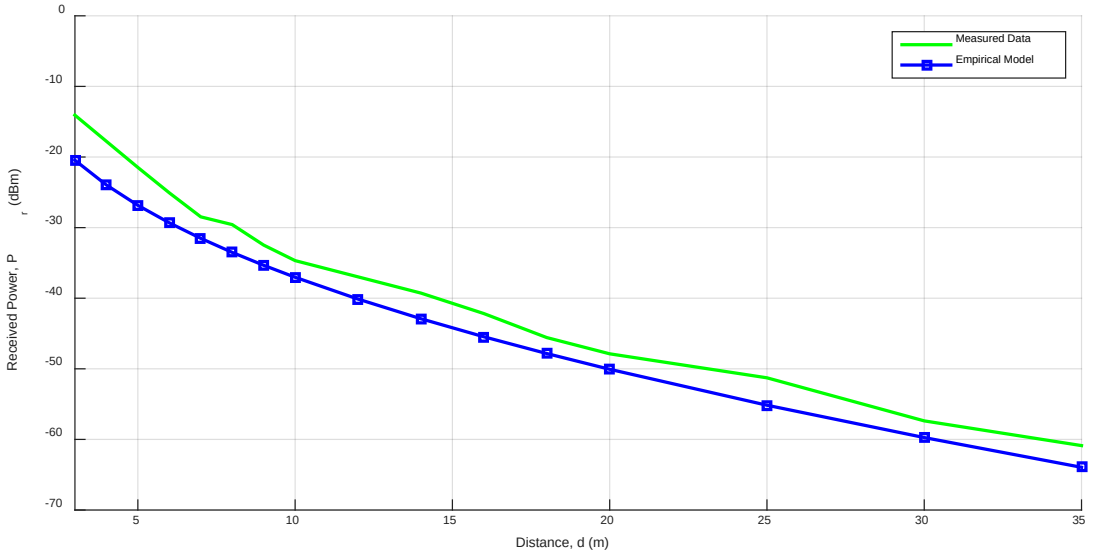

Figure 30. Comparison of the analytical model results versus measured data for horizontally polarized antennas in foliage at 2.0 m.

D. LACK OF POLARIZATION DEPENDENCE

Radio waves become severely depolarized as a result of the interaction with the randomly distributed media. Comparisons between both polarizations sets of measurements are displayed in Figure 31 and Figure 32.

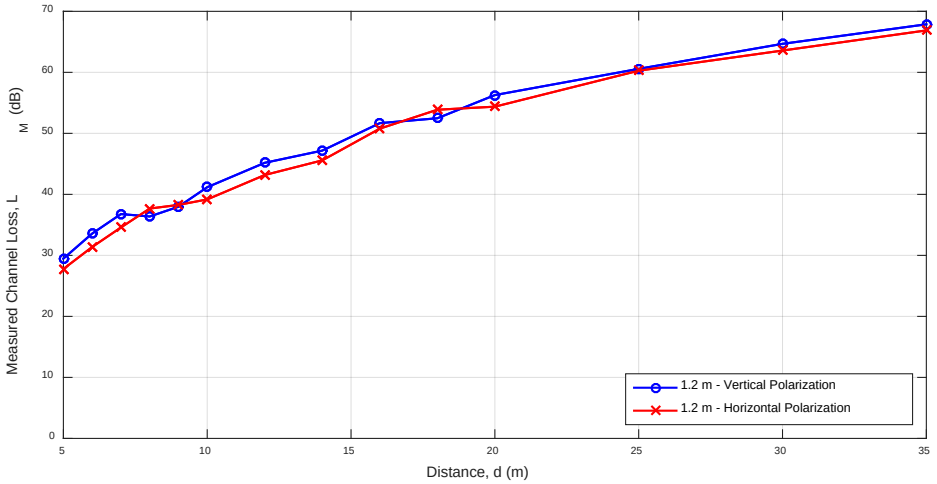

Figure 31. Comparison between vertical and horizontal polarization at 1.2 m.

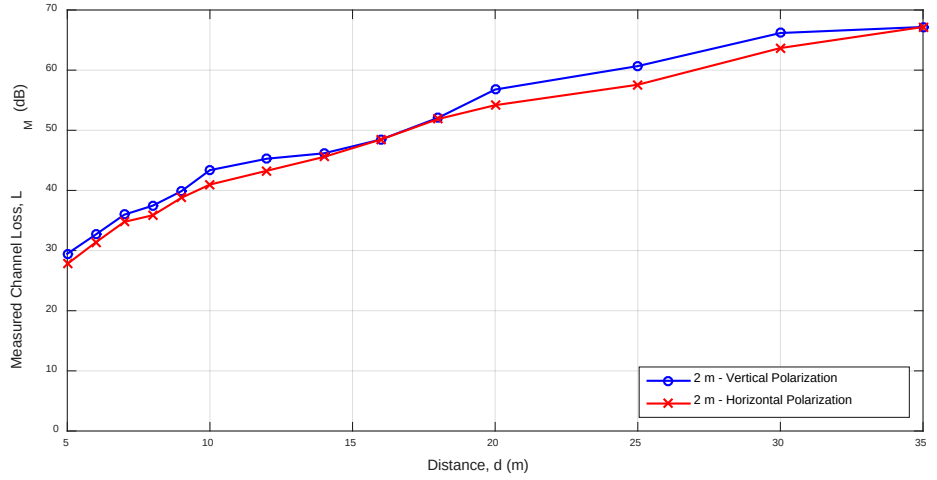

Figure 32. Comparison between vertical and horizontal polarization at 2.0 m.

The depolarization magnitude is closely related to the operational frequency. Because of the orientation of vegetation elements, vertically polarized waves suffer a higher attenuation at low frequencies. Research conducted in [21] showed through measurements that, as frequency increases, the attenuation difference between horizontal and vertically polarized fields decreases.

The new decay prediction model provided a fairly accurate description of excess loss due to foliage for both polarizations. At this operational frequency, the model can estimate losses independently from the polarization because the wavelength interacts equally with horizontal and vertical discrete scatterers in different orientations.

V. ANALYTICAL PATH LOSS MODELING OF PROPAGATION

A. PREVIOUS CONSIDERATIONS AND ASSUMPTIONS

For the analytical modeling, the forest is assumed to be a medium composed of a continuous lossy dielectric representing a group of randomly distributed discrete lossy scatterers. Given that, in terms of wavelengths, the transmitting and receiving antennas were sufficiently far away from the edges of the forested environment where the measurements were taken [15], reflections from edges of the forest are neglected for the modeling phase.

The lateral wave contribution is not considered to be significant because of the operational frequency of the measurements [15]. Also, as was verified during the experimental phase, reflected waves from the forest-air interface do not represent a significant component of the received signal. The vegetation elements at the forest-air interface attenuate the wave because they tend to be larger than the wavelength. Only the direct path and ground-forest components propagating through a dielectric block are considered for the formulation of the deterministic model. The model setup with the remaining contributing mechanisms is depicted in Figure 33.

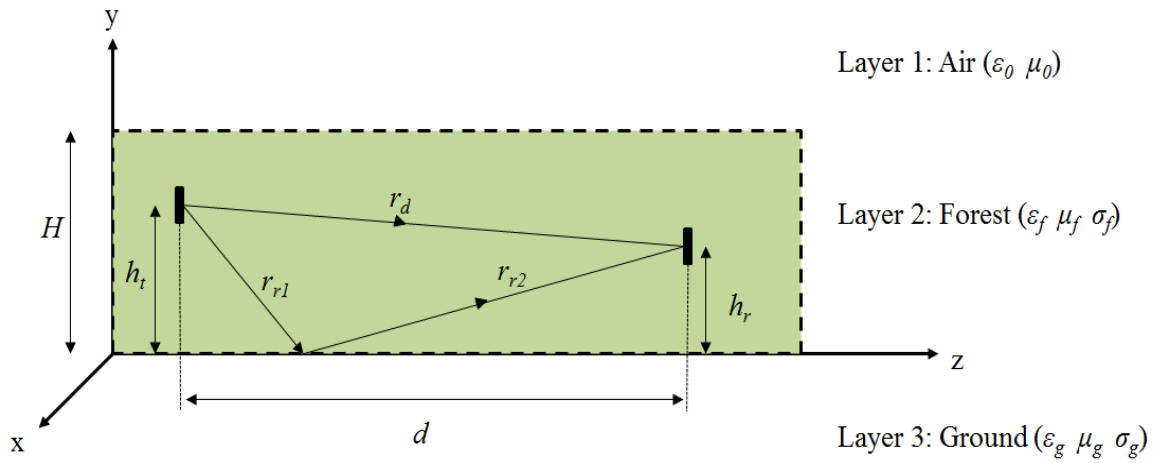

Figure 33. Deterministic propagation model.

B. MODEL FORMULATION

The goal of the analytical model is to provide an accurate, physically based prediction of waves radiating through foliage by adding together the contributions from the direct field and the ground-reflected field at a given observation point. Properties of both GO components were described in Section II.B. Given that effects from the forest-air layer interface are neglected, the model is assumed to be a two-layered model. MATLAB was used to compute the radio wave propagation using Eq. (33).

In the equivalent slab model of the forest, there are two critical parameters that must be defined prior the study of the propagation mechanisms: the relative permittivity and the conductivity of the forest layer. Ranges of foliage parameters stated in [13] were used in Eq. (11) and plotted in Figure 34 to visualize how the attenuation changed as a function of these parameters. Recalling the attenuation value estimated in Section IV.B ($\hat{\alpha}$ = 0.0845 Np/m), all the possible combinations of relative permittivity and conductivity giving this value are contained in Figure 34.

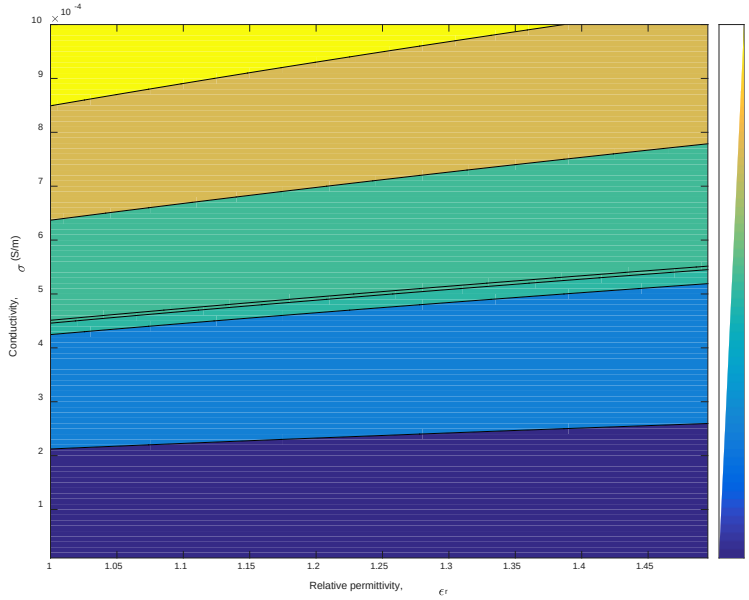

Figure 34. Attenuation constant for combinations of relative permittivity and conductivity.

As can be seen in Figure 34, attenuation increases when either the conductivity increases or the relative permittivity decreases. For the actual computation of the excess attenuation loss L_{att}, the resulting attenuation constant is required rather than specific values of the forest parameters. Using the mid-range values of both parameters ($\hat{\varepsilon}_r = 1.25$ and $\hat{\sigma} = 0.000502$ S/m) gives $\hat{\alpha} = 0.0845$ Np/m. This computation is based on a frequency of 2.4 GHz, so even if experiments are conducted in the same medium, these values may vary as a function of frequency. As frequency increases, the conductivity tends to increase [31]. This may be attributed to a stronger scattering rate given that the anisotropy of the forest becomes more pronounced.

Given one of the main propagation modes of the model is the ground-reflected wave, the electrical properties of the ground are as important as the electrical properties of the foliage. Considering that the terrain of the location where measurements were performed (which serves as reference for the eventual validation of the analytical model) consisted of very dry soil, the corresponding relative permittivity and conductivity for 2.4 GHz according to [14] are $\varepsilon_r = 3.0$ and $\sigma = 0.0015$ S/m. These two parameters are used to calculate the intrinsic impedance η_g of the ground medium with Eq. (27).

After finding η_g, we computed the reflection coefficient of the ground Γ_g. For the simplification of the model, the gains of both transmitting and receiving antennas were set to 14.5 dBi. Both antennas are assumed to be immersed inside the forest layer. Contributions from the lateral wave and forest-air interface are not significant compared to the other mechanisms; therefore, the height of the layer is not required.

Even if it is not directly evident from the modified PGF of Eq. (33), $|F|$ not only varies with distance and attenuation constant but also with antenna height, because this is one of the factors influencing the value of Γ_g. Excess attenuation loss L_{att} was computed by Eq. (34) for the four measured scenarios under evaluation, and the results are plotted in Figure 35 to Figure 38.

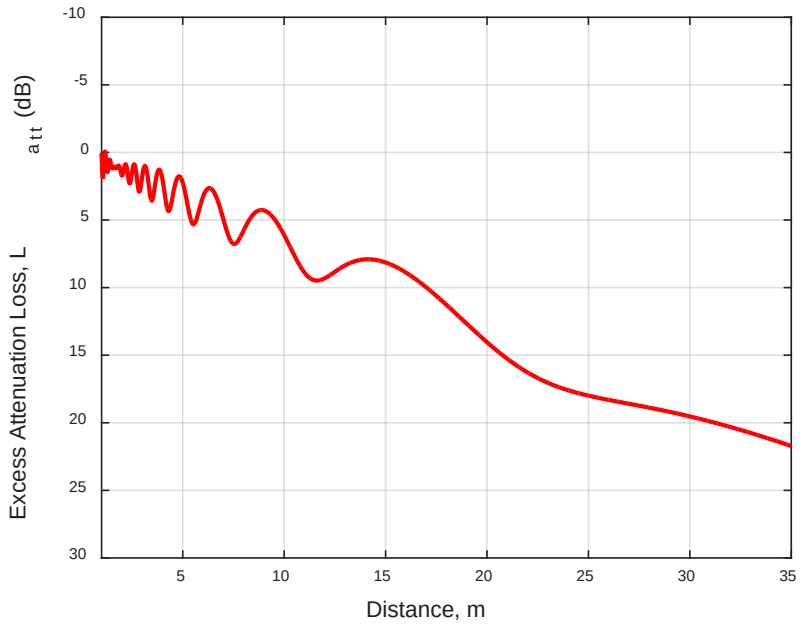

Figure 35. Excess attenuation loss for vertically polarized antenna at 1.2 m immersed in lossy slab with $\hat{\alpha} = 0.0845$ Np/m.

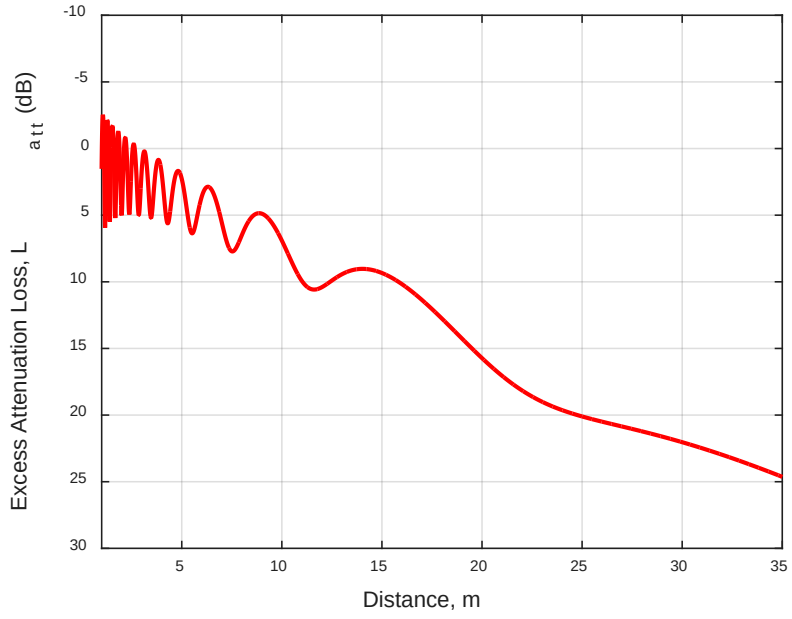

Figure 36. Excess attenuation loss for horizontally polarized antenna at 1.2 m immersed in lossy slab with $\hat{\alpha} = 0.0845$ Np/m.

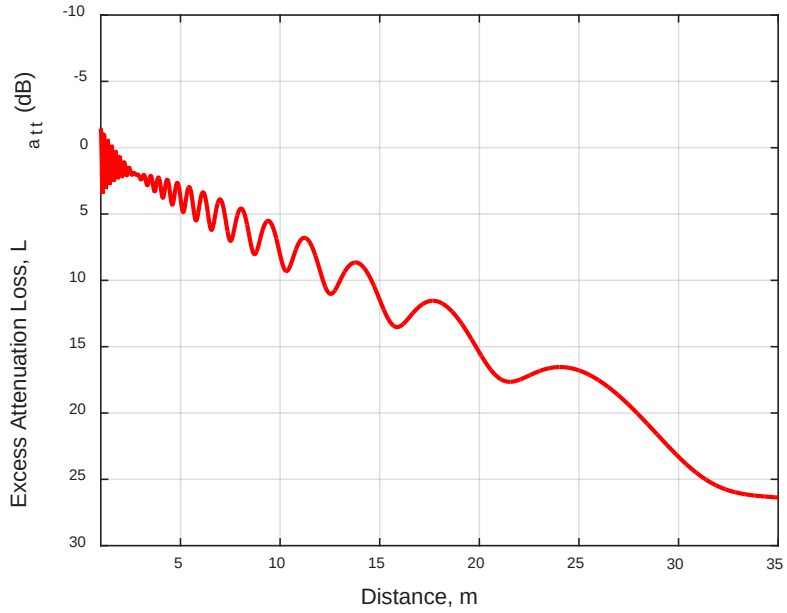

Figure 37. Excess attenuation loss for vertically polarized antenna at 2.0 m immersed in lossy slab with $\hat{\alpha} = 0.0845$ Np/m.

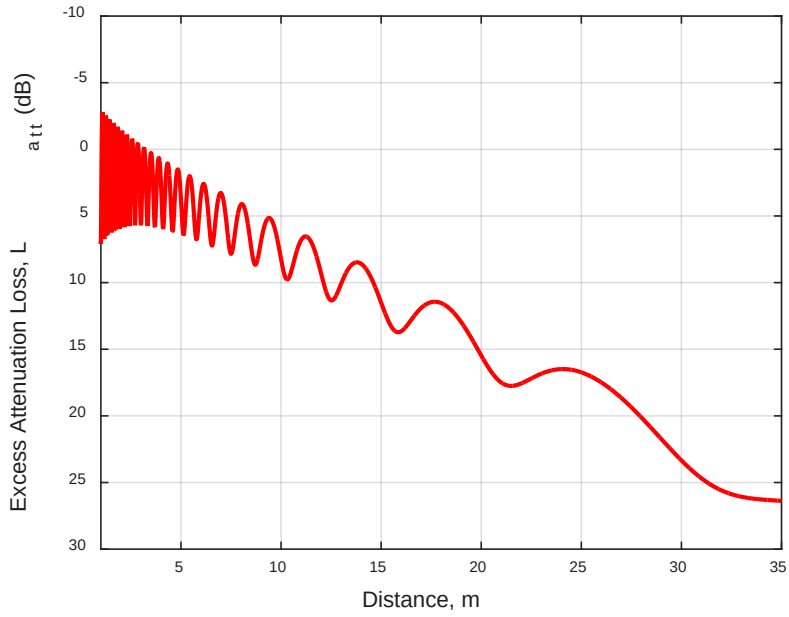

Figure 38. Excess attenuation loss for horizontally polarized antenna at 2.0 m immersed in lossy slab with $\hat{\alpha} = 0.0845$ Np/m.

It is observed that the pattern of the excess attenuation loss depends on the intrinsic impedance of the ground. As long as the relative permittivity and conductivity of the ground layer do not change, the peaks and nulls on the excess attenuation loss remain at the same location if antenna heights are the same in both cases. The decay rate is related to the estimated attenuation constant. It is noticed that as the distance increases, the influence of the attenuation becomes predominant over the effect of the polarization. Also, the antenna heights affect the details of the pattern itself (locations of peaks and nulls) but do not necessarily the decay rate.

C. MODEL EVALUATION

The accuracy of the analytical model was verified through comparison with the experimental data. The formulation of the analytical model must take into account the frequency of the radio wave, the dimension of the object of interaction, and a propagation distance that fulfills the far-field conditions. The foliage depth covered at 2.4 GHz is from 3.0 m to 35.0 m, representing the measured points from the beginning of the far-field until the breakdown of the link. The logarithmic results from Eq. (39) are plotted with the actual measurements in Figure 39 to Figure 42.

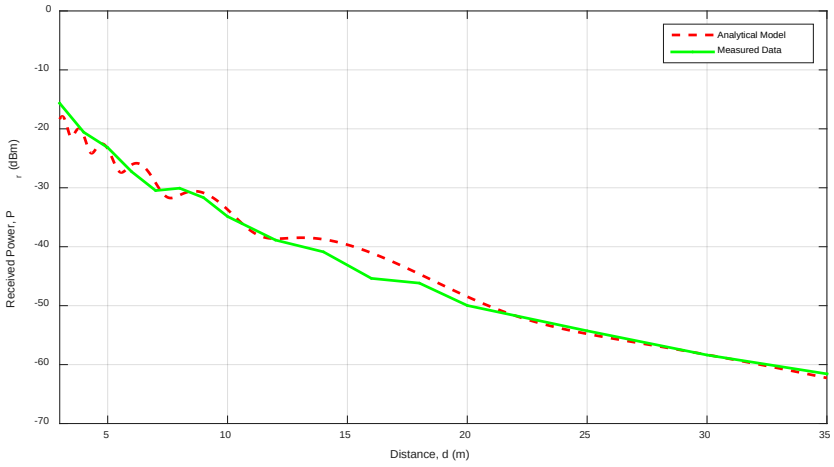

Figure 39. Comparison of the analytical model versus measured data for vertically polarized antennas in foliage at 1.2 m.

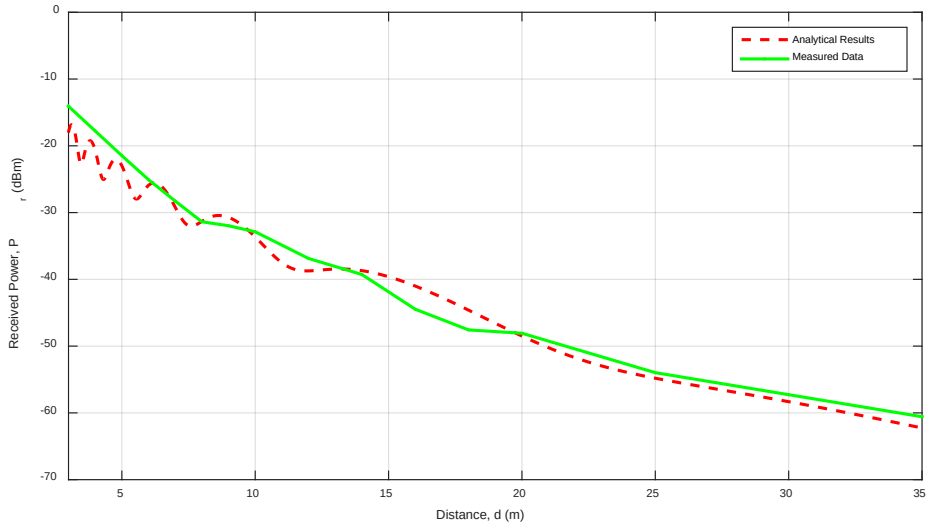

Figure 40. Comparison of the analytical model versus measured data for horizontally polarized antennas in foliage at 1.2 m.

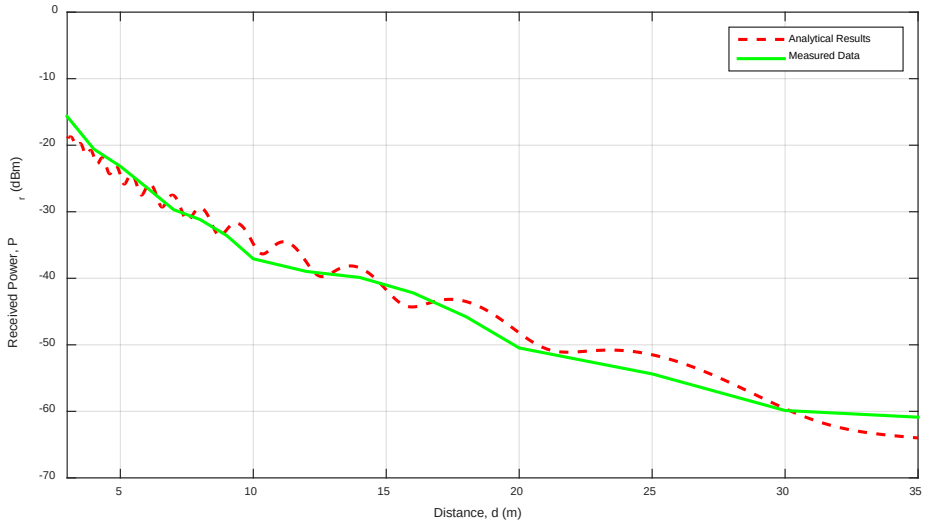

Figure 41. Comparison of the analytical model versus measured data for vertically polarized antennas in foliage at 2.0 m.

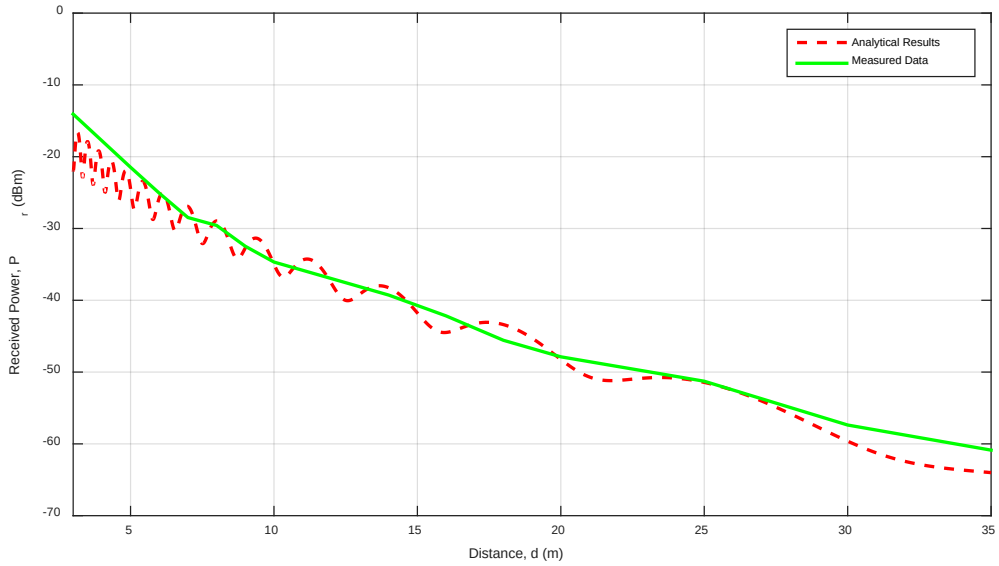

Figure 42. Comparison of the analytical model versus measured data for horizontally polarized antennas in foliage at 2.0 m.

From Figure 39 to Figure 42, we notice that the results of the analytical model are close (generally within 5.0 dB) to the measured, received power. In most of the simulated cases, the predicted received power is slightly higher than the actual measured power. This may be due to the incoherent components inducing a different loss that was not considered in the dielectric slab model. The forest dielectric parameters used in the model may also contribute to the difference. Although it was verified that varying these parameters does not affect the decay rate as long as the attenuation constant remained the same, this may not be applicable in realistic cases.

VI. PATH LOSS MODELING WITH CEM SOFTWARE

A. GENERAL SETUP FOR SIMULATION OF RADIO WAVE PROPAGATION IN FOLIAGE.

In addition to analysis and measurements, a third approach to determine path loss is simulation with CEM software. Modern CEM software can rigorously solve a wide range of problems that include antennas, materials and boundary conditions.

1. General Simulation Approach

Obviously, it is impractical to model the actual geometry of a scenario. A computational model for radiowave propagation in foliage is presented. The foliage is modeled as a lossy dielectric block over conductive ground with similar dimensions of the operational context selected for the experimental procedure. The EM propagation model was characterized via FEKO ®, a commercial CEM software tool for the EM field analysis [32]. For the setup and simulation phase, the computer aided design (CAD) module CADFEKO is utilized, and the simulated results are analyzed with the post-processing module POSTFEKO.

2. Physical Construction

Prior to the dielectric block modeling, scenario characteristics have to be established. Two dielectric materials are defined as shown in Table 6. Dielectric media requires two inputs: relative permittivity ε_r and conductivity σ. These values are combined to result in a complex permittivity as in Eq. (3). For comparison purposes, the values for the “Foliage” and “Ground” dielectric media were the same as those selected for the analytical model in Chapter V.

Table 6. Electrical properties of the simulated media.

Medium	Relative permittivity, ε_r	Conductivity, σ (S/m)
Foliage	1.25	0.000502
Ground	3	0.0015

First, an infinite ground plane was created in the $x-y$ plane and the region $z \leq 0$ given the electrical properties of the "Ground" dielectric medium. A single layer homogenous *Cuboid* object 40.0 m long, 5.0 m wide and 3.0 m tall was constructed to represent the foliage. The cuboid is configured to have the electrical properties of the "Foliage" medium. The constructed scenario is shown in Figure 43.

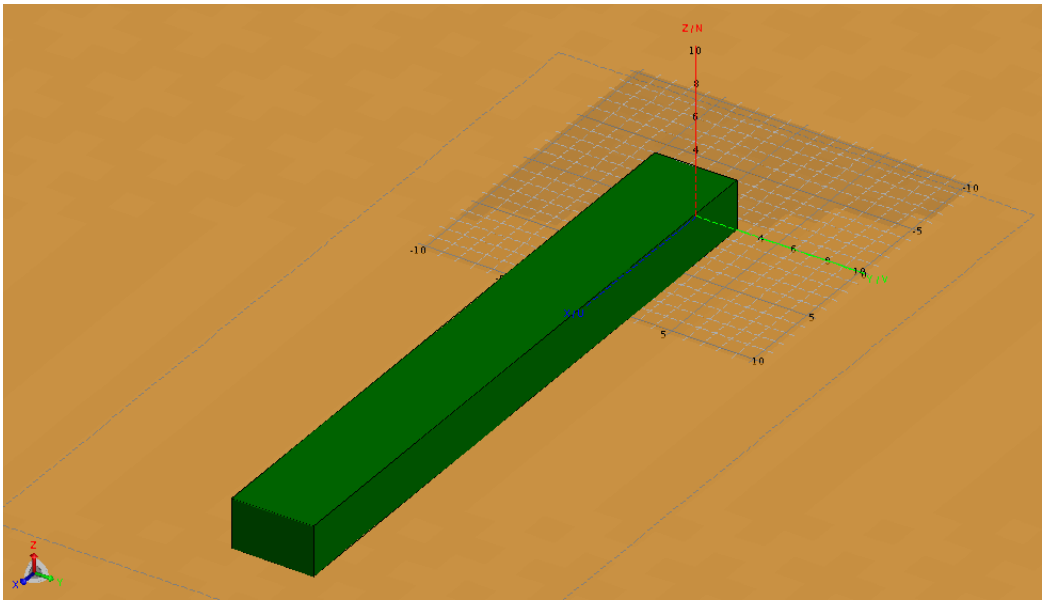

Figure 43. Forest dielectric block constructed in FEKO.

A half-wave dipole antenna was modeled as a thin perfect electric conductor (PEC) rod. The length of the dipole was set to 0.059375 m, slightly less than half the wavelength corresponding to the operational frequency. The radius of the rod was set to 0.000425 m. A "wire port" is placed in the middle of the rod in order to feed the dipole antenna with power for the simulation. The dipole dimensions were selected in order to

match the antenna to 50 Ω. When the antenna is matched, most of the incident energy is radiated because the scattering parameter is low at the frequency of operation. This was verified by requesting an “S-parameter sweep” in FEKO. The frequency range evaluated for the sweep was from 1.0 GHz to 3.0 GHz. The S-parameter sweep generates the return loss results displayed in Figure 44.

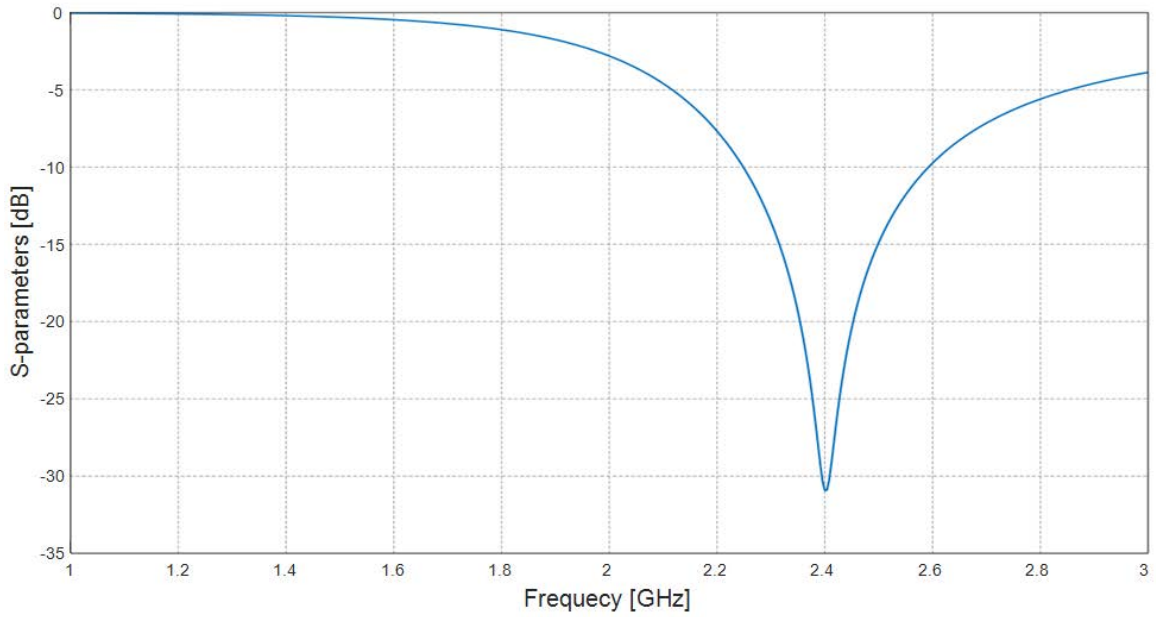

Figure 44. S-parameter result for the selected dimensions of the dipole antenna

The selected dimensions resulted in a minumum at the frequency of interest. Given the reference data that is going to be used to evaluate the simulated model is the measured data, the dipole input power is set as the same power that was used during the experimental phase. Gain differences are accounted for in the post-processing procedure. The dipole was located at the beginning of the foliage block, and its height and polarization depended on the measurement scenario that was simulated.

3. Solution settings

The simulation is solved by means of a full coupling between the method-of-moments (MoM) and physical optics (PO). MoM is a technique used to solve the electric-

field integral equation (EFIE) and the magnetic-field integral equation (MFIE) [33]. The discretization, where the object of interest and its surrounding volume are sliced into small elements, is applied for the numerical analysis of EM radiation and scattering. Given that the foliage block is electrically large compared to the wavelength, the PO approach is formulated on the dielectric boundaries. PO is an asymptotic numerical method used for high frequency applications. Within the dielectric the MoM and the multilevel fast multipole method (MLFMM) with surface equivalent was used [32]. The main drawback as implemented in FEKO was an overwhelming number of meshcells that required significant computational resources and convergence time.

To monitor the fields produced by the simulation, a near-field calculation was requested. Given requested fields and simulation objects cannot overlap with each other, a gap space was inserted in the dielectric block by subtracting a thin *Cuboid* object from the foliage block via *Boolean subtraction* operation in the location of the requested near field. The width of the gap is 0.00125 m (0.01λ).

B. MODEL EVALUATION

The near-field request gives three results: electric field, magnetic field, and Poynting vector. The generated data can be exported as ASCII files and manipulated in MATLAB. Given that the Poynting vector represents the power density [11] (density and direction of power flow at a point), it is possible to find the received power from the Poynting vector at a specific location and the effective area of the receiving antenna. The effective area concept is useful when dealing with antennas in receiving mode. The received power at the antenna terminals is given by the power per unit area carried by incident the field and the effective area of the antenna [19]. The effective area of an antenna A_e is given by

$$A_e = \frac{\lambda^2 G_r}{4\pi} \ . \tag{60}$$

The received power based on the magnitude of the Poynting vector S in W/m^2 and effective area A_e in m^2 is obtained from

$$P_r = SA_e \tag{61}$$

where P_r is the received power in W. The Poynting vector data was exported as ASCII files and processed in MATLAB to generate received power versus distance curves. The logarithmic results from Eq. (61) are plotted with the actual measurements in Figure 45 to Figure 48.

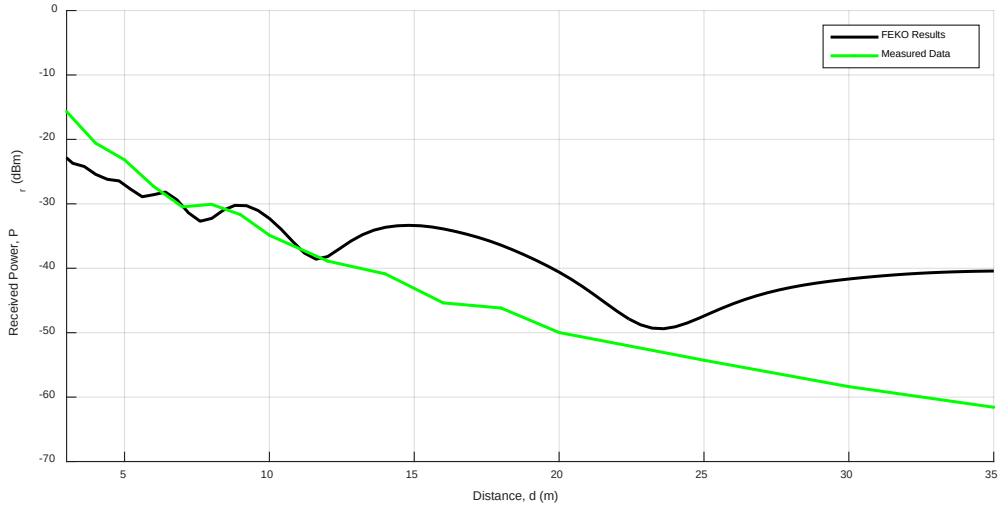

Figure 45. Comparison of results generated by FEKO versus measured data for vertically polarized antennas in foliage at 1.2 m.

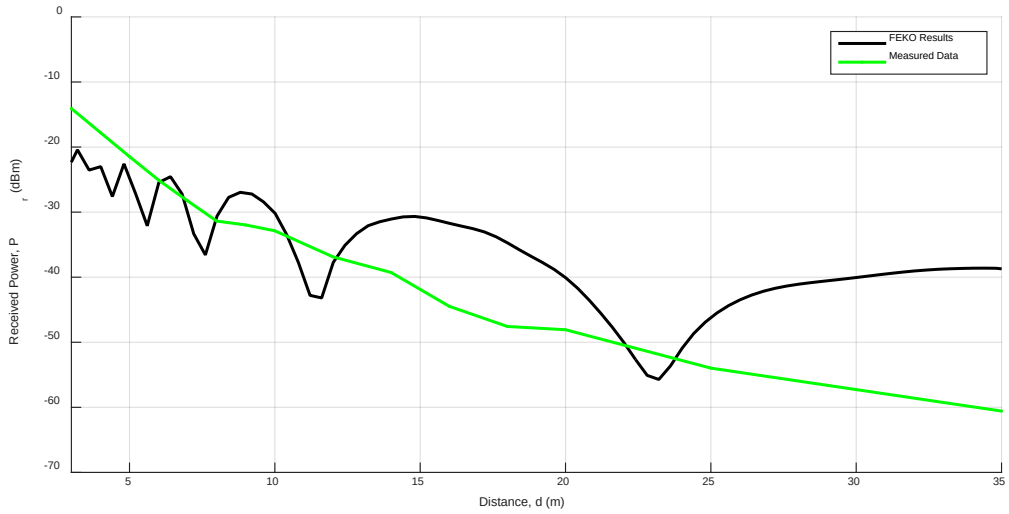

Figure 46. Comparison of results generated by FEKO versus measured data for horizontally polarized antennas in foliage at 1.2 m.

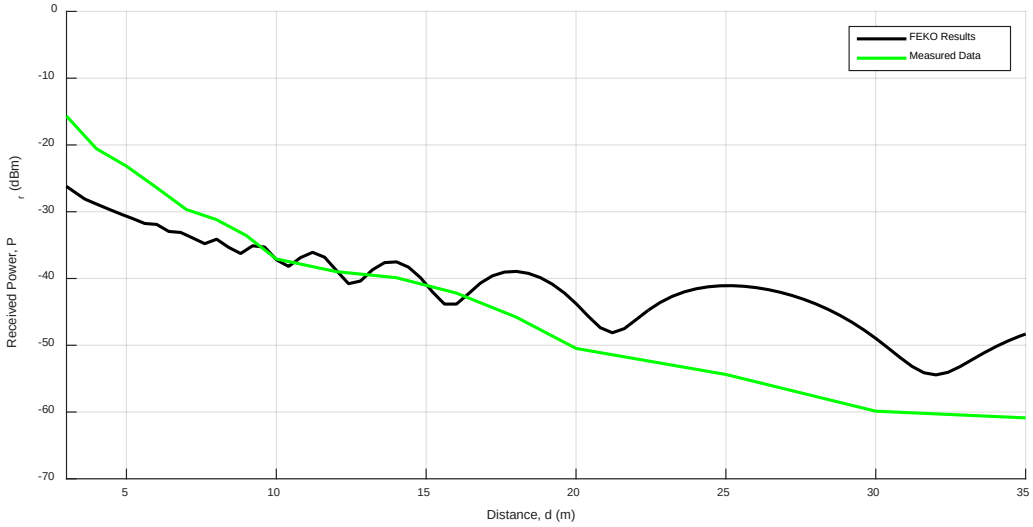

Figure 47. Comparison of results generated by FEKO versus measured data for vertically polarized antennas in foliage at 2.0 m.

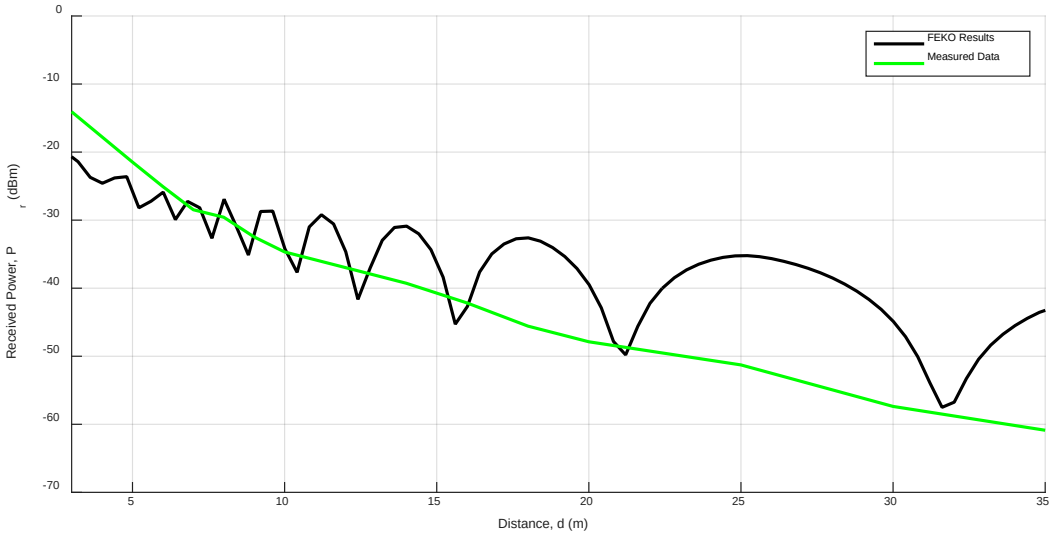

Figure 48. Comparison of results generated by FEKO versus measured data for horizontally polarized antennas in foliage at 2.0 m.

From the various simulations, it is notable that the results generated by FEKO do not closely follow the same pattern as the measured data. Unlike the empirical and the analytical model, the predicted loss produced by the CEM software is much lower than the measured one. Even though both the analytical and FEKO models had the same inputs for relative permittivity and conductivity, which define the decay rate of the received power, the difference between their results does not match. By comparing results from the CEM software simulation model with the analytical model results shown in Figure 39 to Figure 42, we see that the curves have similar loss patterns in terms of location of peaks and nulls, meaning that the simulated scenario with FEKO may give a fair representation of the effects of the ground-reflected wave. The dielectric block may provide a good representation of the actual scenario; however, the features of the antenna (i.e., antenna gain, directivity, radiation pattern) used in the simulation are not the same as those used for the measurements. Even if it was attempted to compensate for these differences in the post-processing section of this model, the magnitude and propagation pattern are still not close enough to state that the results of this simulation can describe the received power in a forested environment or the additional path loss due to foliage.

THIS PAGE INTENTIONALLY LEFT BLANK

VII. SUMMARY, CONCLUSIONS, AND RECOMMENDATIONS

A. SUMMARY

The objective of this research was to develop and evaluate three different approaches to loss prediction due to foliage and compare them with experimental data. Wireless propagation measurements were taken for LOS and obstructed paths in an electrically large dense foliage block for distances up to 35.0 m at different heights. The path loss induced by the presence of vegetation was isolated and fit to an exponential model through the method of nonlinear-least-squares. An attenuation constant was estimated from this fitting. Using only the extracted additional foliage loss, we formulated an empirical model. The performance of the new empirical model was compared to other existing empirical models.

After examining the measured received radio signal, two main propagation mechanisms were identified. The main mechanism in the channel is the forward scattering caused by the randomly distributed vegetation elements obstructing the path between the transmitting and the receiving station. The multipath component associated with reflections from the ground-forest interface also has a significant effect on the overall received signal. The contribution of a possible lateral wave and reflected waves from the forest-air interface were neglected in this analysis. Based on the most important mechanisms, an analytical model representing propagation in a dielectric slab was implemented.

The CEM software FEKO was employed to simulate EM propagation through a single dielectric block that represents the forest. The forest electrical parameters utilized were the same as those used in the analytical model. The model was evaluated at the operational frequency used during the experimental phase. Simulation results were processed with MATLAB to generate received power plots as a function of distance. The suitability of the three proposed models was assesed by comparing their outputs with the measured data.

B. CONCLUSIONS

Prediction models expressing the additional attenuation of vegetation media as a function of path length and frequency are required for the reliable design of communication systems and WSN. In all the cases, foliage increased the signal decay to a certain degree regardless of the antenna polarization and height. The results on the new empirical model showed a better performance than the other models. This was expected because the new model was developed entirely from the experimental data, and the other models were based on different forested scenarios.

The analytical model results were also compared with the experimental data and close agreement was observed. The height of the antenna did not affect the magnitude of the excess loss but does have a major influence over the location of peaks and nulls of the pattern. The contribution of the polarization effects are more pronounced at short distances. In these two scenarios, the horizontally polarized antennas caused a greater amplitude between peaks and nulls before the attenuation effect becomes predominant, showing an almost equal pattern with vertically polarized antennas for longer distances. The plane-Earth loss model overestimated the overall path loss and was not included for the formulation of this model.

The effective medium parameters of the vegetation and ground were found to be strongly influential over the propagation mechanisms. These parameters were estimated to lead to the attenuation constant required for the formulation of the model, and an actual knowledge of them may increase the prediction accuracy of the model. Given that it is not possible to exercise control over these parameters, it is difficult to ascertain any exact relationship between them. Guidelines for determining these parameters have not been reported.

In comparison to the empirical and the analytical model performances, the specific CEM software model used to predict path loss was not adequate. Even though the same relative permittivity and conductivity for foliage and ground were used in both analytical and FEKO, their predicted losses are not close. The difference is attributed to

the approximation made in setting up the simulation model and the numerical and computational approximation used in the solver.

Even though this research provides that the empirical and analytical models are applicable for scenarios with similar features to that in which the experimental data was gathered, their results provide only limited knowledge about the signal interaction with the channel.

C. RECOMMENDATIONS

The role of experimental data based on field measurements is crucial in the development of vegetation excess loss. A greater amount of experimental data, (i.e., different frequencies, antenna heights, separation distance) is required in order to increase the reliability of both the empirical and analytical models formulated herein as well as to gain a better understanding of the channel.

For larger distances than those recorded in this research, there is likely a more noticeable contribution from other mechanisms such as lateral waves and reflected waves from the forest-air interface; hence, their characterization may lead to a highly accurate attenuation prediction. To fully understand and analyze EM wave behavior in forested channels, the non-coherent component produced by vegetation elements scattered and the attenuated direct wave should be separated and, perhaps, modeled independently.

THIS PAGE INTENTIONALLY LEFT BLANK

APPENDIX

In this Appendix, the MATLAB code used to plot additional foliage loss curves as function of distance for the empirical models considered is listed.

```
%% Empirical Models of Propagation in Foliage
% Plot Foliage Loss Predicted by Empirical Models
% written by: Jesus Zegarra, ECE Dept, Naval Postgraduate School.

clear all
close all

% Model inputs
d=input('Distance (m): ');
f=input('Frequency (Hz): ');

% Frequency adjusments
f_MHz=f/1e6;
f_GHz=f/1e9;

D=0:d;

% New model parameters
A=0.18;
B=0.35;
C=0.59;

for ii=1:length(D) % range in meters
 % Weissberger model
 L_weiss(ii)=(1.33*(f_GHz^0.284)*(D(ii)^0.588));

 % ITU model
 L_itu(ii)=(0.2*(f_MHz^0.3)*(D(ii)^0.6));

 % F-ITU model
 L_fitu(ii)=(0.39*(f_MHz^0.39)*(D(ii)^0.25));

 % L-ITU model
 L_litu(ii)=(0.48*(f_MHz^0.43)*(D(ii)^0.13));

 % Seville model
 L_sev(ii)=(0.37*(f_MHz^0.3)*(D(ii)^0.38));

 % COST-235 mode
 L_cost(ii)=(15.6*(f_MHz^-0.009)*(D(ii)^0.26));

 % New Empirical model
 L_new(ii)=(A*(f_MHz^B)*(D(ii)^C));
```

```
end

% Plot loss-distance curves
plot(D,L_weiss,'--','LineWidth',1.5,'Color',[.0 .0 .8]);
hold on
plot(D,L_itu,'--','LineWidth',1.5,'Color',[.0 .8 .0]);
plot(D,L_fitu,'--','LineWidth',1.5,'Color',[.8 .0 .0]);
plot(D,L_litu,'--','LineWidth',1.5,'Color',[.0 .8 .8]);
plot(D,L_sev,'--','LineWidth',1.5,'Color',[.8 .0 .8]);
plot(D,L_cost,'--','LineWidth',1.5,'Color',[.8 .8 .0]);
plot(D,L_new,'LineWidth',1.5,'Color',[.0 .0 .0]);

axis([1 max(D) -1 50])
h_legend= legend('Weissberger model','ITU-R model','FITU-R model','L-ITU model','Seville
model','COST 235 model','New model','Location','SouthEast');
set(h_legend,'FontSize',12);
xlabel('Distance (m)','FontSize',14)
ylabel('Measured Excess Path Loss, L_f_o_l_i_a_g_e (dB)','FontSize',14)
grid on
```

MATLAB code used to plot the received power as a function of distance for propagation through foliage predicted by the new empirical model.

```
%% Empirical Model for Propagation in Foliage
% Calculate Empirical loss due to foliage and modify Friis Equation
% written by: Jesus Zegarra, ECE Dept, Naval Postgraduate School.

clear all
close all

% Model inputs
d=input('Distance (m): ');
f=input('Frequency (Hz): ');
Pt=input('Transmitted power (Watts): ');
Gtdb=input('Transmitter antenna gain (dB): ');
Grdb=input('Receiving antenna gain (dB): ');

% Regresion results
f_MHz=f/1e6;
A=0.12;
B=0.35;
C=0.75;

D=0:0.01:d;

% Antennas' features
lambda=3e8/f;
Gt=db2pow(Gtdb);
Gr=db2pow(Grdb);

for ii=1:length(D) % range in meters
  L_emp_new(ii)=((A*(f_MHz^B)*(D(ii)^C)));
  Pr_Friis(ii)=(Pt*Gt*Gr*(lambda^2))/((4*pi*D(ii))^2); %Friss equation
```

```
  Prdbm_Emp(ii)=(pow2db(Pr_Friis(ii)))+30-(L_emp_new(ii));
end

% Plot excess attenuation loss
figure(1)
plot(D,L_emp_new,'-r','Linewidth',2)
set(gca,'Ydir','reverse')
xlabel('Distance, m','FontSize',14)
ylabel('Excess Attenuation Loss, L_a_t_t (dB)','FontSize',14)
grid on
axis([1,35,-10,30])

% Plot Received power
figure(2)
plot(D,Prdbm_Emp,'-b','Linewidth',2)
grid on
axis([1 max(D) -70 0])
xlabel('Distance, d (m)')
ylabel('Received Power, P_r (dBm)')
```

MATLAB code used to plot the received power as a function of distance for propagation through foliage predicted by the analytical model.

```
%% Analytical Model for Propagation in Foliage
% Plot Excess Attenuation Loss and Received Power versus Distance Curves
% written by: Jesus Zegarra, ECE Dept, Naval Postgraduate School.

clear all
close all

% Model inputs
d=input('Distance (m): ');
f=input('Frequency (Hz): ');
Pt=input('Transmitted power (Watts): ');
Gtdb=input('Transmitter antenna gain (dB): ');
Grdb=input('Receiving antenna gain (dB): ');
ht=input('Transmitter antenna height (m): ');
hr=input('Receiver antenna height (m): ');
eps_r_g=input('Ground relative permittivity: ');
sigma_g=input('Ground conductivity (S/m): ');
eps_r=input('Foliage relative permittivity: ');
sigma=input('Foliage conductivity (S/m): ');
pol_s=input('Select Polarization (V or H): ','s');

% Wavelength and wavenumber
lambda=3e8/f;
k=2*pi/lambda;
w=2*pi*f;

% Free space permittivity, permeability and conductivity
eta0=120*pi;
```

```
mu0=4*pi*1e-7;
eps0=8.853*1e-12;

% Ground intrinsic impedance
eta_g=sqrt((mu0)/(eps0*eps_r_g*(1-(j*(sigma_g/(eps0*eps_r_g*w))))));

% Foliage intrinsic impedance and attenuation constat
eta_r=sqrt((mu0)/(eps0*eps_r*(1-(j*(sigma/(eps0*eps_r*w))))));
alpha=w*sqrt((mu0*eps0*eps_r/2)*((sqrt(1+((sigma/(w*eps0*eps_r))^2)))-1));

% Ground reflection
D=0:0.01:d;
for it=1:length(D)
  bp(it)= D(it)/(1+(ht/hr)); % Reflection point
  theta_i(it)=atand(ht/bp(it));
  theta_t(it)=asind((sind(theta_i(it)))/(sqrt(eps_r_g)));
  gamma_g_v(it)=((eta_g*cosd(theta_t(it)))-
(eta_r*cosd(theta_i(it))))/((eta_g*cosd(theta_t(it)))+(eta_r*cosd(theta_i(it)))); % complex reflection
coefficient of ground
  gamma_g_h(it)=((eta_g*cosd(theta_i(it)))-
(eta_r*cosd(theta_t(it))))/((eta_g*cosd(theta_i(it)))+(eta_r*cosd(theta_t(it)))); % complex reflection
coefficient of ground
end

% Polarization selection
if pol_s=='V';
  gamma_g=gamma_g_v;
elseif pol_s=='H';
  gamma_g=gamma_g_h;
end

% Antennas' features
Gt=db2pow(Gtdb);
Gr=db2pow(Grdb);

for ii=0:(length(D)-1) % range in meters
  ii=ii+1;
  R0(ii)=sqrt(D(ii)^2+(hr-ht)^2);
  R12(ii)=sqrt(D(ii)^2+(hr+ht)^2);
  dR(ii)=R12(ii)-R0(ii);
% PGF direct + reflected with loss
  F0(ii)=abs(exp(-alpha*R0(ii))+gamma_g(ii)*exp(-j*k*dR(ii))*exp(-alpha*R12(ii)));
  F0db(ii)=-20*log10(F0(ii));
  Pr(ii)=Pt*Gt*Gr*lambda^2/(4*pi*D(ii))^2*F0(ii)^2;
  Prdb(ii)=10*log10(Pr(ii));
  Prdbm(ii)=Prdb(ii)+30;
end

% Plot excess attenuation loss
figure(1)
plot(D,F0db,'-r','Linewidth',2)
set(gca,'Ydir','reverse')
xlabel('Distance, m','FontSize',14)
```

```
ylabel('Excess Attenuation Loss, L_a_t_t (dB)','FontSize',14)
grid on
axis([1,35,-10,30])

% Plot Received power
figure(2)
plot(D,Prdbm,'-b','Linewidth',2')
grid on
axis([1 max(D) -70 0])
xlabel('Distance, d (m)')
ylabel('Received Power, P_r (dBm)')
```

MATLAB code used to plot the received power as a function of distance for propagation through foliage predicted by the CEM software model.

```
%% CEM Software Model for Propagation in Foliage
% Plot FEKO Received Power versus Distance Curves
% POSTFEKO provides data as matrices containing Poynting vector values in
% W/m^2 with a correspondent distance in m.
% written by: Jesus Zegarra, ECE Dept, Naval Postgraduate School.

clear all
close all

% Load data from POSTFEKO files
filename=input('Enter Poynting vector FEKO file name: ','s');
FEKO=importdata(filename,'-mat');

% Model inputs
f=input('Frequency (Hz): '); % Frequency has to be the same as the one used
% as input frequency in FEKO
Gtdb=input('Transmitter antenna gain (dB): ');
Grdb=input('Receiving antenna gain (dB): ');

% Set distances and Poynting vector
D_Feko=(FEKO(:,1))';
S_Feko=FEKO(:,2);

% Frequency and Antennas' features
lambda=3e8/f;
Gt=db2pow(Gtdb);
Gr=db2pow(Grdb);
Ae=(Gr*(lambda^2))/(4*pi); % Effective area

Pr_Feko=S_Feko.*Ae*Gt; % Calculate Received power in Watt

Prdb_Feko=10*log10(Pr_Feko);
Prdbm_Feko=Prdb_Feko+30;

figure(1)
```

```
plot(D_Feko,Prdbm_Feko,'-k','Linewidth',2)
axis([1 max(D_Feko) (min(Prdbm_Feko)-5) 0])
grid on
xlabel('Distance, d (m)')
ylabel('Received Power, P_r (dBm)')
```

MATLAB code used to plot the plane-Earth loss predicted loss as a function of distance and antenna height.

```
%% Plane-Earth Model
% Plot plane-Earth Model Losses as a function of distance and antenna
% heights. Note that the transmitting antenna is held at a fixed height and
% the losses are computed for different observation points.
% written by: Jesus Zegarra, ECE Dept, Naval Postgraduate School.

clear all
close all

% Model inputs
d=input('Distance (m): ');
f=input('Frequency (Hz): ');
Pt=input('Transmitted power (Watts): ');
Gtdb=input('Transmitter antenna gain (dB): ');
Grdb=input('Receiving antenna gain (dB): ');
ht=input('Transmitter antenna height (m): ');
H=input('Maximum height for observation point (m): ');

% Free space constants
mu0=4*pi*1e-7;
eps0=8.85e-12;
c=physconst('LightSpeed');
lambda=c/f;
w=2*pi*f;

% Antennas' features
Gtdb=1;
Gt=10^(Gtdb/10);
Gr=Gt;

% Scenario features
dr=[0:0.1:d]+0.1;
Nd=length(dr);

hr=[0:0.1:H]+0.1;
Nh=length(hr);

% loop in range (d) and height (h)

for i=1:Nd
  for n=1:Nh
    L_pe(i,n)=((((2*pi*dr(i))^2)))/(Gt*Gr*(lambda^2)*(sind(2*pi*ht*hr(n)/(lambda*dr(i))))^2);
    L_pe_db(i,n)=20*log10(L_pe(i,n));
  end % end of height loop
```

```
end  % end of distance loop

% Plot the loss computed by plane-Earth model
figure(1)
clf
[D1,H1]=meshgrid(dr,hr);
Dmax=max(max(D1));
Hmax=max(max(H1));
Hmin=min(min(H1));
contourf(D1,H1,L_pe_db')
axis([0 Dmax (Hmin+0.2) (Hmax+0.2)]);
hold on
plot(0.1,ht,'g*')
plot([0 Dmax],[H H],'k--')
c = colorbar;
c.Label.String = 'Plane-Earth Loss, L_P_E (dB)';
c.FontSize=12;
xlabel('Distance, d (m)')
ylabel('Transmitting and Receiving Antennas Height, h (m)')
```

MATLAB code used to plot attenuation as a function of relative permittivity and conductivity of the medium.

```
%% Dielectric slab attenuation diagram
% Attenuation constant is computed as a function of input values of
% relative permittivity, conductivity and frequency.
% written by: Jesus Zegarra, ECE Dept, Naval Postgraduate School.

clear all
close all

% Model inputs
f=input('Frequency (Hz): ');
eps_r_min=input('Lower limit of dielectric relative permittivity: ');
eps_r_max=input('Upper limit of dielectric relative permittivity: ');
sigma_min=input('Lower limit of dielectric conductivity (S/m): ');
sigma_max=input('Upper limit of dielectric conudctivity (S/m): ');


% Free space constants
mu0=4*pi*1e-7;
eps0=8.85e-12;
c=physconst('LightSpeed');
lambda=c/f;
w=2*pi*f;

% Propagation media
N=1000; % number of points for dielectric variables
eps_r=linspace(eps_r_min,eps_r_max,N);
ee=length(eps_r);
sigma=linspace(sigma_min,sigma_max,N);
ss=length(sigma);
```

```
% Attenuation and Phase constants
for ii=1:ee
  for jj=1:ss
    alpha(ii,jj)=w*sqrt((mu0*eps0*eps_r(ii)/2)*((sqrt(1+((sigma(jj)/(w*eps0*eps_r(ii)))^2)))-1));
    beta(ii,jj)=w*sqrt((mu0*eps0*eps_r(ii)/2)*((sqrt(1+((sigma(jj)/(w*eps0*eps_r(ii)))^2)))+1));
  end % end of relative permittivity loop
end % end of conductivity loop

% Plot attenuation constant results (alpha)

figure(1)
[L1,H1]=meshgrid(eps_r,sigma);
contourf(L1,H1,alpha')
c = colorbar;
c.Label.String = 'Attenuation, \alpha (Np/m)';
c.FontSize=12;
hold on
xlabel('Relative permittivity, \epsilon_r')
ylabel('Conductivity, \sigma (S/m)')
```

MATLAB function developed to perform a non-linear least-square based on input data.

```
function [scale, alpha, rmse, Qpre] = expFit(D, data)
% Exponential fit based on non-linear least-squares method

% Remove offset
No_off=data-min(data);

% Fitting
[xData, yData] = prepareCurveData( D, No_off );

% Set up fittype and options.
%(a*exp(-b*x))/(x^2)
ft = fittype( 'a*exp(-b*x)', 'independent', 'x', 'dependent', 'y');
opts = fitoptions( 'Method', 'NonlinearLeastSquares' );
opts.Display = 'Off';
opts.StartPoint = [1 0.5];

% Fit model to data.
[fitresult, gof] = fit( xData, yData, ft, opts );

scale=fitresult.a;
alpha=fitresult.b;

rmse=gof.rmse;

Qpre=scale.*exp(-alpha.*D)+min(data);
end
```

LIST OF REFERENCES

[1] C. R. Anderson, H. I. Volos, W. C. Headley, F. Mueller, and R. M. Buehrer, "Low-antenna ultrawideband propagation measurements and modeling in a forest environment," in *Proc. IEEE Wireless Commun. Netw. Conf.*, 2008, pp. 1229–1234.

[2] Y. S. Meng, Y. H. Lee, and B. C Ng, "Study of propagation loss prediction in forest environment," *Progress in Electromagn. Res. B*, vol. 17, pp. 117–133, 2009.

[3] *Atlas of Australian Resources*, vol.6, Australian Surveying and Land Information Group, Canberra, Australia, 1990.

[4] T. Tamir, "On radio wave propagation in forest environments," *IEEE Trans. On Antennas Propag*., vol. AP-31, no. 6, pp. 806–817, November 1967.

[5] G. P. D. S. Cavalcante, D. A. Rogers, and A. J. Giardola, "Radio loss in forest using a model with four layered media," *Radio Sci.*, vol. 18, no. 5, pp. 691–695, 1983.

[6] G. S. Brown and W. J. Curry, "A theory and model for wave propagation through foliage," *Radio Sci.*, vol. 17, no. 5, pp. 1027–1036, September/October 1982.

[7] G. G. Joshi, C. B. Dietrich, C. R. Anderson, W. G. Newhall, W.A. Davis, J. Isaacs and G. Barnett, "Near-ground channel measurements over line-of-sight and forested paths," *Proc. Inst. Elect. Eng. Microw. Antennas Propag.*, vol. 152, no. 6, pp. 589–596, December 2005.

[8] A. Seville and K. H. Cragi, "Semi-empirical model for millimeter-wave vegetation attenuation rates," *Electron. Lett.*, vol. 31, no. 17, pp. 1507–1508, 1995.

[9] Y. C. Lin and K. Sarabandi, "A monte carlo coherent scattering model for forest canopies using fractal-generated trees," *IEEE Trans. Geosci. Remote Sensing*, vol. 37, no.1, pp. 440–451, January 1999.

[10] C. A. Lewis, J. T. Johnson, and F. L. Teixeira, *Radiowave Propagation*, John Wiley & Sons, Hoboken, New Jersey, 2010.

[11] F. T. Ulaby, E. Michielssen, and U. Ravaioli, *Fundamental of Applied Electromagnetics*, 6th ed., Prentice Hall, Upper Saddle River, New Jersey, 2010.

[12] R. K. Tewari, S. Swarup, and M. N. Roy, "Evaluation of relative permittivity and conductivity of forest slab from experimentally data on lateral wave attenuation constant," *Int. J. Electron.*, vol. 61, no 5, pp 597–605, 1986.

[13] G. H. Hagn and H. W. Parker, “Feasibility study of the use of open-wire transmission lines, capacitors and cavities to measure the electrical properties of vegetation,” Stanford Research Institute, Special Tech. Rept. 13, August 1966.

[14] ITU-R Recommendation P.527-3, “Electrical characteristics of the surface of the Earth,” International Telecommunications Union, 1992.

[15] T. Tamir, “Radio waves propagation along mixed paths in forest environments,” *IEEE Trans. Antennas Propag.*, vol. AP-25, pp. 471–477, July 1977

[16] G. P. S. Cavalcante, D. A. Rogers, and A. J. Giardola, “Radio loss in forests using a model with four layered media,” *IEE Proc. Microw. Antennas Propag.*, vol. 134, no. 4, pp. 361–368, 1987.

[17] S. S. Seker, “Radio pulse transmission along mixed paths in a stratified forest,” *IEE Proc. Microw. Antennas Propag.*, vol. 136, no. 1, pp. 13–18, 1989.

[18] S. Haykin and M. Moher, *Introduction to Analog & Digital Communications*, 2nd ed., John Wiley & Sons, Hoboken, New Jersey, 2007.

[19] J. D. Parsons, *The Mobile Radio Propagation Channel*, 2nd ed., John Wiley & Sons, Hoboken, New Jersey, 2000.

[20] M. Pozar, *Microwave Engineering*, 4th ed., John Wiley & Sons, Hoboken, New Jersey, 2012.

[21] M. A. Weissberger, “An initial critical summary of models for predicting the attenuation of radio waves by foliage,” *Electromagnetic Compatibility Anal. Center*, Annapolis, MD, ECAC-TR-81-101, 1981.

[22] CCIR, “Influence of terrain irregularities and vegetation on troposphere propagation,” CCIR Report, 235–236, Geneva, 1986.

[23] M. O. Al-Nuaimi and R. B. L Stephens, “Measurements and prediction model optimization for signal attenuation in vegetation media at centimeter wave frequencies,” *IEE Proc. Microw. Antennas Propag.*, vol. 145, no. 3, pp. 201–206, 1998.

[24] Y. S. Meng, Y. H. Lee, and B. Ng, “Empirical near ground path loss modeling in a forest at VHF and UHF,” *IEEE Trans. On Antennas Propag.*, vol. 57, no. 5, pp. 1461–1468, 2009.

[25] COST 235, “Radio propagation effects on next-generation fixed-service terrestrial communications systems,” Final Report, Luxembourg, 1996.

[26] J. Goldman and G. W. Swenson, “Radio Wave Propagation through woods,” *IEEE Antennas Propag. Magazine*, vol. 41, no. 5, pp. 34–37, 1999.

[27] S. Swarup and R. K. Tewari, “Depolarization of radio waves in jungle environment,” *IEEE Trans. Antennas Propag.*, vol. 27, no. 1, pp. 113–116, 1979.

[28] L-com, Inc., “HyperLink Wireless 2.4 GHz 14.5 dBi Radome Enclosed Wireless LAN Yagi Antenna,” HG2415Y datasheet.

[29] W. L. Stutzman and G. A. Thiele, *Antenna Theory and Design*, 3th ed., John Wiley & Sons, Hoboken, New Jersey, 2013.

[30] Y. Li and H. Ling, “Numerical modeling and mechanism analysis of VHF wave propagation in forested environments using the equivalent slab model,” *Progress in Electromag. Res.*, vol. 91, pp. 1734, 2009.

[31] L. W. Li, T. S. Yeo, P. S. Kooi, and M. S. Leong, “Radiowave propagation along mixed paths through a four-layered model of rain forest: an analytical approach,” *IEEE Trans. Antennas Propagat.*, vol. 46, no. 7, pp. 10981111, 1998.

[32] FEKO. (July 31, 2015). [Online]. Overview of FEKO. https://www.feko.info/product-detail/overview-of-feko.

[33] I. V. Lindell, *Methods for Electromagnetic Field Analysis*, 1st ed., IEEE Press, New Jersey, 1995.

THIS PAGE INTENTIONALLY LEFT BLANK

INITIAL DISTRIBUTION LIST

1. Defense Technical Information Center
   Ft. Belvoir, Virginia

2. Dudley Knox Library
   Naval Postgraduate School
   Monterey, California